

Period-luminosity and period-luminosity-metallicity relations for Galactic RR Lyrae stars in the Sloan bands[★]

W. Narloch¹, G. Hajdu¹, G. Pietrzyński¹, W. Gieren², B. Zgirski², P. Wielgórski¹, P. Karczmarek², M. Górski¹,
and D. Graczyk³

¹ Nicolaus Copernicus Astronomical Center, Polish Academy of Sciences, Bartycka 18, 00-716 Warszawa, Poland
e-mail: wnarloch@camk.edu.pl

² Universidad de Concepción, Departamento de Astronomía, Casilla 160-C, Concepción, Chile

³ Nicolaus Copernicus Astronomical Center, Polish Academy of Sciences, Rabiańska 8, 87-100 Toruń, Poland

Received ..., 2024; accepted ..., 2024

ABSTRACT

Context. RR Lyrae stars are excellent tracers of the old population II due to their period-luminosity (PL) and period-luminosity-metallicity (PLZ) relations. While these relations have been investigated in detail in many photometric bands, there are few comprehensive studies about them in Sloan-like systems.

Aims. We present PL and PLZ relations (as well as their counterparts in Wesenheit magnitudes) in the Sloan–Pan-STARSS $g_{P1}r_{P1}i_{P1}$ bands obtained for Galactic RR Lyrae stars in the vicinity of the Sun.

Methods. The data used in this paper were collected with the network of 40 cm telescopes of the Las Cumbres Observatory, and geometric parallaxes were adopted from Gaia Data Release 3.

Results. We derived PL and PLZ relations separately for RRab and RRc-type stars, as well as for the mixed population of RRab+RRc stars.

Conclusions. To our knowledge, these are the first PL and PLZ relations in the Sloan bands determined using RR Lyrae stars in the Galactic field.

Key words. distance scale – Sloan: stars – Stars: variables: RR Lyrae – Galaxy: solar neighborhood – galaxies: Milky Way

1. Introduction

RR Lyrae-type stars (hereafter RR Lyr stars) are low-mass radially pulsating giants of the horizontal branch on the Hertzsprung-Russell (HR) diagram. Initially, since they were mostly discovered in globular clusters, they also used to be referred to as cluster-type variables (e.g., Bailey 1902; Bailey & Pickering 1913), but they were also found in the Galactic field (e.g., Kapteyn 1890), including the star RR Lyr (Pickering 1901), which eventually became the prototype of this class of variables. Originally, they were divided by Bailey (1902) into three subclasses (a, b and c), today simplified into just two: ab and c, where RRab stars are known to be fundamental mode pulsators, while RRc stars are pulsating in the radial first-overtone. Much later RRd stars were introduced into the nomenclature, (e.g., Jerzykiewicz & Wenzel 1977; Sandage et al. 1981; Nemec 1985) being double-mode pulsators, pulsating simultaneously in both fundamental and first-overtone modes, as well as RRe stars (e.g., Demers & Wehlau 1977) pulsating in the second-overtone only.

Because of the similarities between RR Lyr stars and Cepheids, Shapley (1918) incorporated them into his calibration of the Cepheid period-luminosity (PL) relation and used it as a tool for measuring distances to Galactic globular clus-

ters which, in turn, he used to estimate the distance to the center of the Milky Way (MW). This has proven the usefulness of the RR Lyr stars as distance indicators, which over time became one of the most important standard candles, besides Cepheids. Despite the fact that RR Lyr stars are fainter than Cepheid variables, they serve as distance indicators to old population II stars, where young Cepheids are not observed, such as: globular clusters (e.g., ω Centauri from Navarrete et al. 2017; Braga et al. 2018) and dwarf galaxies (e.g., Sculptor dSph, Carina, and Fornax galaxies from Pietrzyński et al. 2008; Karczmarek et al. 2015, 2017). The near-infrared (NIR) PL relations of RR Lyr stars are of particular interest, as they are very well defined and characterized with a small scatter (e.g., Zgirski et al. 2023; Bhardwaj et al. 2023; Bhardwaj 2024). The amplitudes of the NIR light curves of the RR Lyr stars are smaller than in the optical domain, and the shapes are much more sinusoidal, so accurate mean magnitudes can be estimated from only a few photometric points. Moreover, the reddening in the NIR is almost negligible. In the optical regime, the PL relations for RR Lyr stars are characterized by almost flat relations, dominated by the dependence on the metallicity (see, e.g., Cáceres & Catelan 2008), so their usefulness for distance determinations is of less importance, compared to NIR. Nevertheless, the existing large-scale sky surveys, such as the Sloan Digital Sky Survey (SDSS; Abazajian et al. 2003) or the upcoming 10 yr Vera C. Rubin Observatory Legacy Survey of Space and Time (Rubin-LSST; Ivezić et al. 2019), use wide-band Sloan photometric filters (*ugriz*; Fukugita et al. 1996), so there appeared to be an urgent need to provide a precise calibra-

[★] Based on data from the Las Cumbres Observatory. The light curves are only available in electronic form at the Araucaria Project webpage: <https://arucaria.camk.edu.pl/> and the CDS via anonymous ftp to cdsarc.u-strasbg.fr (130.79.128.5) or via <http://cdsweb.u-strasbg.fr/cgi-bin/qcat?J/A+A/>.

tion of the PL relations in those filters to effectively take advantage of these data sets.

This need was addressed by studies from both the theoretical and observational sides. On the one side, in their noteworthy works, Marconi et al. (2006) and Cáceres & Catelan (2008), presented their theoretical period-magnitude-color and PL relations, respectively, for RR Lyr stars, calculated in the *ugriz* SDSS photometric system. More recently, Marconi et al. (2022) published theoretical period-luminosity-metallicity (PLZ) relations for RR Lyr stars in the Rubin-LSST filter system. The empirical calibrations in the Sloan bands were done mostly using RR Lyr in globular clusters. Sesar et al. (2017) published PLZ relations in the *griz* bands, using the first data release from the Panoramic Survey Telescope And Rapid Response System (Pan-STARSS1, Kaiser et al. 2010) based on the RR Lyr stars from five globular clusters. Vivas et al. (2017) published empirical PL relations for the *ugriz* filter set of the Dark Energy Camera (DECAM, Flaugher et al. 2015) for RR Lyr variables from the globular cluster M5. Bhardwaj et al. (2021) determined PL relations in the *gi* bands for RR Lyr stars from the globular cluster M15, using data gathered with the 3.6 m Canada–France–Hawaii Telescope (CFHT) and calibrated to the SDSS photometric system. Ngeow et al. (2022), on the other hand, used data from the Zwicky Transient Facility (ZTF; Bellm et al. 2018; Bellm et al. 2019; Dekany et al. 2020) in the Sloan *gri* bands to derive the PLZ and period-Wesenheit-metallicity (PWZ) relations based on hundreds of RR Lyr stars from 46 globular clusters. To the best of our knowledge, the empirical PL relations in the Sloan passbands for RR Lyr stars from the vicinity of the Sun have not been determined so far. Deriving them by taking advantage of very high-quality geometric parallaxes provided by the Gaia mission (Gaia Collaboration et al. 2023) would be an important contribution to this field.

Our aim in this work is to calibrate the PL and PLZ relations (as well as their counterparts in the Wesenheit magnitudes which are reddening-free by construction; Madore 1982) for the MW RR Lyr stars in the three Sloan *gri* bands, and specifically as they are implemented in the Pan-STARSS photometric system (Tonry et al. 2018), similarly as we did in the case of the Galactic classical Cepheids in Narloch et al. (2023). By this, we expect to provide a useful tool to determine distances in the universe, given the upcoming era of the ambitious programs such as the Rubin-LSST.

The paper is organized as follows. In Section 2 we provide a description of the data and reduction process, as well as methods of calculation of absolute magnitudes, and source of metallicities of our stars. In Section 3 we describe the derivation of the PL and PW, and PLZ and PWZ relations, which we further discuss in Section 4. A short Summary in Section 5 concludes the paper.

2. Data

2.1. Sample of stars

We have observed 53 RR Lyr type stars in total, among them 44 fundamental mode stars (hereafter RRab) and nine first overtone stars (hereafter RRc). The stars are bright with Gaia G-magnitudes in the range from 8.97 to 12.87 mag and they are distributed all over the sky, however, with the majority located in the southern hemisphere. The range of distances calculated as the inverse of the Gaia Data Release 3 (DR3) parallaxes (Gaia Collaboration et al. 2023) is between ≈ 0.5 and ≈ 2.9 kpc, with a median distance of about 1 kpc. The sky distribution of the

analyzed RR Lyr stars is shown in Figure 1, where circles denote RRab and squares RRc stars. The pulsational periods of our sample stars were adopted from the International Variable Star Index¹ (AAVSO) and range between about 0.36 and 0.88 days. The physical parameters of stars are summarized in Table 1.

2.2. Data and reduction

Data for the project were collected between 2021 August and 2022 July with 16 robotic 40 cm telescopes of the Las Cumbres Observatory (LCO) Global Telescope Network² within observing programs CLN2021B-008 and CLN2022A-008. Images were obtained in the Sloan *g'r'i'* filters using 3K \times 2K SBIG STL-6303 cameras with field of view 29.2×19.5 arcmin², and a pixel size of 0.571 arcsec pixel⁻¹ without binning. The air mass range was 1.0–1.6, and average seeing was about 2.35, 2.28 and 2.30 arcsec in the Sloan *g*, *r* and *i* bands, respectively.

We downloaded images already reduced and processed with the LCO BANZAI³ pipeline from the LCO Archive⁴. The aperture photometry and calibration of data was done the same way as in Narloch et al. (2023), which we recommend to see for details of the procedure. The mean DAOPHOT photometric uncertainties were ≈ 0.03 mag for the Sloan *g* filter and ≈ 0.02 mag for Sloan *ri* filters for all stars with Sloan *g* < 14.0 mag, which is the range of magnitudes from which most of the reference stars are from. The average photometric error for the range of magnitudes of the RR Lyr stars from our sample ($9.0 < g < 13.0$ mag) was about 0.01 mag in all three filters.

The influence of the nonlinearity of the LCO SBIG cameras was not as severe in case of the RR Lyr stars as it was in case of classical Cepheids in Narloch et al. (2023), as we were using photometric calibration reference stars with brightnesses similar to the target stars. Nevertheless, we applied exactly the same calibration equations as in Narloch et al. (2023) to account for that effect.

The final intensity-averaged mean apparent magnitudes obtained by fitting the Fourier series to the RR Lyr stars light curves are expressed in the photometric system of the ATLAS All-Sky Stellar Reference Catalog version 2 (ATLAS-REFCAT2; Tonry et al. 2018), which is in the Pan-STARSS system (Tonry et al. 2012) referred to as $g_{P1}r_{P1}i_{P1}$ later in the text. The applied Fourier order ranged between 2 and 13, where the higher Fourier orders were used to better fit the maximum brightness of specific cases. Figures A.1 and A.2 present the final light curves of our RRab and RRc stars, respectively⁵.

2.3. Reddening

To deredden our data we used the E(B-V) color excess values from Schlafly & Finkbeiner (2011), available for all RR Lyr stars from our sample, and integrated up to the distance of our targets assuming the three-dimensional MW model of Drimmel & Spergel (2001) (for details of the adopted model parameters see, e.g., Suchomska et al. 2015). The extinction vectors (R_i) for the Sloan–Pan-STARSS $g_{P1}r_{P1}i_{P1}$ bands were adopted from Green et al. (2019, see their Table 1), and they are equal to $R_g = 3.518$,

¹ <https://www.aavso.org/vsx/>

² <https://lco.global/>

³ <https://lco.global/documentation/data/BANZAIpipeline/>

⁴ <https://archive.lco.global/>

⁵ The light curves are available at the webpage of Araucaria Project: <https://araucaria.camk.edu.pl/> and the CDS.

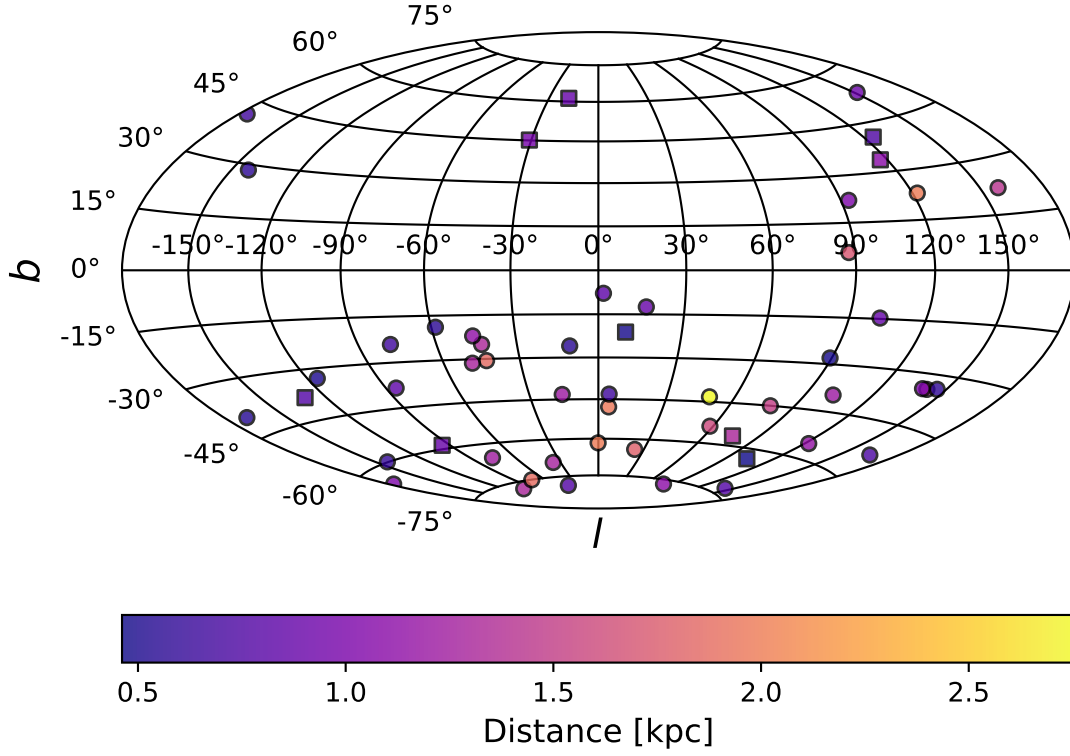


Fig. 1. Location of the RR Lyr stars (RRab, circles; RRC, squares) on the sky used for establishing the PL relations in this paper given in Galactic coordinates.

$R_r = 2.617$ and $R_i = 1.971$. We used these values to calculate three Wesenheit indices, reddening-free by the construction (for a specific reddening law, Madore 1982), and we defined $W_r^{ri} = r - 4.051(r - i) - \mu$, $W_r^{sr} = r - 2.905(g - r) - \mu$, and $W_g^{gi} = g - 2.274(g - i) - \mu$, where μ is a distance modulus (DM).

2.4. Distances

We applied four different techniques to determine the absolute magnitudes (M_λ) calculated from the mean apparent magnitudes (m_λ) of RR Lyr stars from our sample:

- Classical method, where we adopted the geometric parallaxes from the Gaia DR3 catalog and corrected for the zero point (ZP) offset proposed by Lindegren et al. (2021)⁶ and inserted them directly into the following formula:

$$M_\lambda = m_\lambda + 5 \log_{10} \varpi + 5, \quad (1)$$

where ϖ is a parallax expressed in arcsec.

- Astrometry-Based Luminosity (ABL; Feast & Catchpole 1997; Arenou & Luri 1999) to avoid the bias in the absolute magnitude caused by its nonlinear relation with the parallax:

$$ABL_\lambda = 10^{0.2M_\lambda} = \varpi_{(arcsec)} \frac{10^{\frac{m_\lambda+5}{5}}}{5}. \quad (2)$$

⁶ We calculated the parallax ZP offset corrections using the dedicated Python code provided for that purpose: https://gitlab.com/icc-ub/public/gaiadr3_zeropoint.

- Geometric distances from Bailer-Jones et al. (2021) derived from Gaia parallaxes using the parallax with a direction-dependent prior on distance:

$$M_\lambda = m_\lambda - 5 \log_{10} r + 5, \quad (3)$$

where r is a distance in pc.

- Photogeometric distances from Bailer-Jones et al. (2021), which were calculated using additional priors on the color and apparent magnitude of a star, where the absolute magnitude can be calculated based on Equation (3).

The Gaia parallaxes for our RR Lyr stars corrected for the ZP offset derived by Lindegren et al. (2021) range between 0.36 and 2.17 mas (see column 3 in Table 1), with a median of 0.99 mas, while the corrections range from about -5 to $-57 \mu\text{as}$ (with a mean of about $-30 \mu\text{as}$). Lindegren et al. (2021) recommended to include an uncertainty of a few μas in the ZP, so we adopted $5 \mu\text{as}$ as a systematic error.

We rejected eight stars in total which did not meet our criteria for the parallax quality, that is, having $\text{RUWE} > 1.4$ or $\text{GOF} > 12.5$, which we adopted after Breuval et al. (2021) and Wielgórski et al. (2022). Because of the sensitivity of the RUWE parameter to photocentric motion of unresolved objects, it might be an indicator of astrometric binaries. The GOF parameter is used as an indicator of the level of asymmetry of a source by, for example, Riess et al. (2021). Six RRab stars from our sample have $\text{RUWE} > 1.4$ (BB Eri, BT Aqr, DH Hya, RV Phe, SZ Gem,

VW Scl; marked with a-symbol in Table 1), among which only four characterize with $GOF > 12.5$. From RRc stars two were rejected based on the RUWE (MT Tel, RU Psc) and none based on the GOF parameter, meaning that the RUWE indicator is more selective in our case.

Eight of our RRab and two of RRc stars fall into the problematic magnitude range of $G = 11.0 \pm 0.2$ mag, where a transition of Gaia window classes occurs (see Figure 1 in Lindegren et al. 2021), where the parallax ZP could be affected. Another five RRab stars fall into the range of $G = 12.0 \pm 0.2$ mag. To account for possible additional errors caused by this, we quadratically added $10 \mu\text{as}$ to the parallax uncertainties of those stars, following Breuval et al. (2021). Finally, all Gaia DR3 parallax errors were increased by 10%, as suggested by Riess et al. (2021) to account for a possible excess uncertainty. The mean parallax uncertainty for our RR Lyr stars given in column 3 of Table 1 is about $20 \mu\text{as}$.

2.5. Metallicities

For the purpose of derivation of the PLZ and PWZ relations we adopted the metallicity values calculated from high-resolution spectra by Crestani et al. (2021b,a). Crestani et al. (2021b) provide the metallicity for 32 RRab and four RRc stars from our sample, while Crestani et al. (2021a) complete this list with another five RRab and one RRc stars (see column 10 of Table 1). We lack the metallicity values from high-resolution spectroscopy for the remaining seven RRab and four RRc stars (see column 11 of Table 1). Nevertheless, we have decided not to adopt them from other sources, to assure a similar quality of the used values, but rather exclude those stars from further analysis of the PLZ and PWZ relations. Metallicities for remaining RRab stars have a wide range from -0.03 to -2.59 dex, with the mean of about -1.40 dex, while the metallicity range for RRc stars is from -1.49 to -2.60 dex, with the mean of -1.93 dex.

3. Derived relations

3.1. Period-luminosity relations

We derived the PL relations for the MW RR Lyr stars using absolute magnitudes in the three Sloan–Pan–STARSS $g_{P1}r_{P1}i_{P1}$ bands with all four methods listed in Section 2.4. For the absolute magnitudes calculated from Equation (1) using the Gaia DR3 parallaxes and Equation (3) using distances from Bailer-Jones et al. (2021) we fit the linear relation:

$$M_{\lambda} = a_{\lambda}(\log P - \log P_0) + b_{\lambda}, \quad (4)$$

where a_{λ} and b_{λ} are the searched slope and intercept. The logarithm of a pivot period ($\log P_0$) is subtracted in order to minimize correlation between the two parameters. Following Zgirski et al. (2023), we set it to be $\log P_0 = -0.25$ in case of the RRab and mixed population of RRab+RRc stars, and $\log P_0 = -0.45$ for RRc stars, where RRc stars were fundamentalized according to the recipe from Iben (1974), $\log P_{RRab} = \log P_{RRc} + 0.127$.

For the absolute magnitudes calculated with the ABL method given by Equation (2) we fit the following relation:

$$ABL_{\lambda} = 10^{0.2[a_{\lambda}(\log P - \log P_0) + b_{\lambda}]}. \quad (5)$$

We performed the fitting of above relations using the `curve_fit` function from the `scipy` Python library with 3σ

clipping. The fitted coefficients for all four methods with the corresponding statistical uncertainties taken as errors returned by the fitting procedure are given in Table 2. They all agree well within their 1σ uncertainty. Figure 2 presents the resulting PL relations with the absolute magnitudes calculated using Gaia DR3 parallaxes, where the error bars are the uncertainties derived from the error propagation based on the statistical errors on the mean magnitudes and parallaxes.

The PL relations derived using four different methods result in almost identical rms, and the obtained coefficients agree well within their 1σ uncertainty. Therefore, on this basis we cannot determine which method is the most reliable one for distance calculation. For the presentation of the results, we decided on the conceptually simplest and most direct method of inverted parallaxes, which we also recommend to use for the distance calculation purposes. Nevertheless, we have included the coefficients for each of the method so that the reader could use them depending on their preferences.

In case of the PL relations for RRab stars, 38 stars were used for the fit. Their distances ranged from about 0.48 to 2.76 kpc, with a median of about 0.97 kpc. The final rms of the fitted relations is 0.18 for all four methods in the Sloan–Pan–STARSS g_{P1} band, and 0.14 – 0.15 in the r_{P1} and 0.13 in the i_{P1} band. In case of the PL relations for RRc variables, 7 stars were used for the fitting only, from the range of distances between 0.46 to 1.31 kpc, with a median ≈ 0.88 kpc. The final rms is 0.11 for the g_{P1} , 0.10 for the r_{P1} and 0.09 – 0.10 for the i_{P1} band. In case of the mixed population, 45 stars were used from the full distance range from 0.46 to 2.76 kpc, with a median of 0.92 kpc. The obtained rms is larger than for the RRab and RRc populations separately, and are 0.21, 0.17 and 0.15 for the Sloan–Pan–STARSS $g_{P1}r_{P1}i_{P1}$ bands, respectively.

3.2. Period-Wesenheit relations

We also performed the fitting using the Wesenheit indices (W_r^{ri} , W_r^{gr} , W_g^{gi}) as defined in Section 2.3 and applying equations analogous to Equations (4) and (5):

$$W = a(\log P - \log P_0) + b, \quad (6)$$

$$ABL_W = 10^{0.2[a(\log P - \log P_0) + b]}, \quad (7)$$

where a and b are the slope and intercept we are looking for and $\log P_0$ is the logarithm of the pivot period as adopted in Section 3.1.

For the fit of the PW relations we used the same number of stars as in the case of the PL relations (38 RRab, seven RRc and 45 RRab+RRc stars). The only exceptions were W_r^{gr} and W_g^{gi} calculated based on photo-geometric distances from Bailer-Jones et al. (2021) where 44 stars were used for the mixed population, as CP Aqr was rejected from the fit after 3σ -clipping. The rms of fitted relations are between 0.10 – 0.12 for RRab, 0.07 – 0.10 for RRc and 0.09 – 0.12 for RRab+RRc stars. The final coefficients are given in Table 2 and the resulting relations for distances calculated based on Gaia parallaxes are presented in Figure 3.

3.3. Period-luminosity-metallicity relations

We performed the fitting of the PLZ relations using the metallicities from Crestani et al. (2021b,a) for 42 of our stars (37 RRab

and four RRc stars, see Section 2.5). After application of selection criteria for RUWE and GOF we were left with 31 RRab and only four RRc. Because of the small number of the latter we decided not to perform the PLZ relation fitting for RRc stars, however, we used them to fit the relations for the mixed population after prior recalculation of their $\log P$ to the fundamental ones (see Section 3.1). We used equations similar to Equations (4)–(7) but extended by the metallicity term in the form:

$$M_\lambda = a_\lambda(\log P - \log P_0) + b_\lambda + c_\lambda([\text{Fe}/\text{H}] - [\text{Fe}/\text{H}]_0), \quad (8)$$

$$ABL_\lambda = 10^{0.2[a_\lambda(\log P - \log P_0) + b_\lambda + c_\lambda([\text{Fe}/\text{H}] - [\text{Fe}/\text{H}]_0)]}, \quad (9)$$

where the new coefficient c_λ is the metallicity slope and $[\text{Fe}/\text{H}]_0$ is the pivot metallicity, chosen to be -1.5 dex, a value close to our median metallicity. We performed the fitting for all four methods of distance calculation. The resulting coefficients for the Sloan *gri* bands and Wesenheit magnitudes with their corresponding errors calculated as in Section 3.1 are given in Table 3. Figure (4a) presents the residuals of the fit for the parallax method for RRab stars and Fig. (4b) the same for mixed population.

The c_λ coefficient values obtained for all four methods of the determination of the absolute magnitudes are within the 1σ uncertainties of each other. The metallicity slopes in the Sloan-Pan-STARRS $g_{p1}r_{p1}i_{p1}$ bands are quite significant (about 0.2 to 0.3 mag/dex) and they decrease toward longer wavelengths. Our values show up to ≈ 0.1 mag/dex larger metallicity dependence than the metallicity slopes obtained by Ngeow et al. (2022, see their Table 4), but the trend is similar. The resulting c_λ values for Wesenheit indices, on the other hand, are smaller than 0.1 mag/dex, being largest for W_r^{ri} and smallest for W_r^{sr} . In comparison, the coefficients from Ngeow et al. (2022) are up to ≈ 0.1 mag/dex larger in this case, although still show a similar trend.

4. Discussion

4.1. Fundamentalization

As indicated in Section 3.1, we fundamentalized the sample of RRc stars using the recipe from Iben (1974) which is simply shifting the $\log P$ of RRc stars by a constant value (0.127 in this case). This method is supposed to align RRc with RRab stars and is commonly used in the literature (e.g., Ngeow et al. 2022; Zgirski et al. 2023). The main reasons behind derivation of PL and PLZ relations (and their Wesenheit versions) for mixed population of RRab+RRc stars is to increase the number of stars used for the fitting, but also in order to compare the results with theoretical predictions (such as Cáceres & Catelan 2008). The latter does not differentiate between RRab and RRc stars as it is difficult to separate them on the HR diagram where their instability strips overlap with each other (see for example Fig. 4 from Kolláth et al. 2002).

However, a simple shift in $\log P$ might not be enough to correctly align those two types of variables. As already noticed by, for instance, Zgirski et al. (2023) in NIR data, and what is also visible in our results based on the Sloan-Pan-STARRS $g_{p1}r_{p1}i_{p1}$ bands (see Tables 2 and 3), the slopes of the relations for both types of RR Lyr stars are different, with slopes of RRc stars being flatter than RRab. After fundamentalization of RRc stars, the PL and PLZ relations for mixed population resulted in even

flatter slopes than for RRab and RRc stars, separately. This is mostly a consequence of existing misalignment. Zgirski et al. (2023) determined new $\log P$ shifts for their sample of stars in *JHK_s* bands. We decided to follow their method of simultaneous $\Delta \log P$ fitting, despite small number of RRc stars (seven and four for PL and PW, and PLZ and PWZ relations, respectively). We obtained the shifts presented in Table 4. The shift values are higher for bluer passbands, which is most probably an effect of flatter slopes in shorter wavelengths, as the shift in $\log P$ -axis is constant. The applied method minimizes the systematic error coming from the classical fundamentalization formula, but does not solve the problem.

The constant value of $\Delta \log P$ from $\log P_{RRab} = \log P_{RRc} + \Delta \log P$ fundamentalization formula was originally derived from pulsational models, from the ratio of the period of the fundamental to the first-overtone modes at the intersection of blue edges of the instability strips for those two modes (Iben & Huchra 1971). After discovery of the classical RRd type stars (Jerzykiewicz & Wenzel 1977), the ratio of the first-overtone to the fundamental period in those stars became the source of the shift value (e.g., Catelan 2009), which agreed remarkably well with the original one. However, as can be seen clearly in Nemeč et al. (2024) this ratio is not constant, but change nonlinearly with period (see their Fig. 1 and Equation 4). So it seems that more correct approach to the fundamentalization would be to apply this nonlinear relation (see Figure 4 in Nemeč et al. 2024) and shift RRc stars according to it. The obtained $\Delta \log P$ values for stars from our sample ranged between 0.128 – 0.153 (with a mean of ≈ 0.133). After recalculation of the PL and PLZ relations, the slopes indeed became slightly steeper, however, the change was well within 1σ uncertainties. The intercept, on the other hand, was not affected. So it turns out that a simple shift by $\Delta \log P = 0.127$ is a sufficient approximation in our case, after all.

Nevertheless, the procedure of fundamentalization of the RRc stars introduces a systematic error into the derived PL and PLZ relations. The luminosities of RRab stars are generally overestimated, which influences the distances determined using such equations. As we showed in Table 4, this bias will depend on the used filter. Although the shift in $\log P$ -axis is constant, the slopes of PL and PLZ relations are different in different bands. We provided the coefficients for PL and PLZ relations for the mixed population in Tables 2 and 3, but for the distance determination purposes we recommend to use the relations for RRab and RRc populations separately.

4.2. The influence of the parallax ZP on the PL and PLZ relations

For the purpose of derivation of our PL and PLZ relations (and their Wesenheit versions) we first corrected Gaia parallaxes for the ZP offset based on Lindegren et al. (2021, see Section 2.4), particularly for parallax and ABL methods, as the geometric and photogeometric distances from Bailer-Jones et al. (2021) have these corrections already incorporated. To check the influence of that value on our results we performed two control tests. First, we have not introduced the corrections at all, and secondly we calculated the corrections according to the prescription given by Groenewegen (2021), where the new mean value was again about $-30 \mu\text{as}$ as for the Lindegren et al. (2021, see Section 2.4). In both cases the slopes for derived PL and PLZ (and Wesenheit) relations, as well as metallicity slope for the PLZ relation agreed well within 1σ uncertainties. In case of the ZPs of the relations, they again agreed very well with parallax corrections determined

based on Groenewegen (2021), but the difference was significant when no corrections were applied. The shift of the intercept values of the PL and PW relations was about 0.07 mag for RRab and 0.05 mag for RRC stars, with intercepts being smaller when no parallax corrections are applied. The difference in those two numbers might come from the fact that RRC stars from our sample are located on average closer to us than RRab stars, so the uncertainty coming from parallax ZP has a smaller influence on them. The ZP shift of the PLZ relations was even slightly larger (about 0.08 mag) when no ZP offset corrections were applied.

4.3. Comparison of the PL and PLZ relations with the literature

The general trend of the slopes of our PL and PLZ relations follows the trends also presented in the results of other works such as Vivas et al. (2017); Ngeow et al. (2022) in the Sloan bands or Zgirski et al. (2023) for NIR data. The slopes of the relations become steeper toward longer wavelengths while the metallicity slopes flatten at the same time. Also, the PL and PLZ relations are better constrained for longer wavelengths, as their dispersion decreases in redder filters. The slopes of PLZ relations for RRab stars are steeper than for RRab+RRC stars, which again was observed in the Sloan passbands by, for example, Ngeow et al. (2022). The direct comparison of our results with different authors is difficult to perform for several reasons. Nevertheless, in the following Sections we present the comparison with the existing PLZ relations, both theoretical and empirical.

4.3.1. Comparison with theoretical PLZ relation

Cáceres & Catelan (2008) presented a theoretical study of the RR Lyr PLZ relation in the *ugriz* SDSS filter system. They provided the PLZ relation in the SDSS *i* band as:

$$M_i = 0.908 - 1.035 \log P + 0.220 \log Z \quad (10)$$

where $\log Z$ can be calculated as:

$$\log Z = [\text{Fe}/\text{H}] + \log(0.638 \times 10^{[\alpha/\text{Fe}]} + 0.362) - 1.765 \quad (11)$$

As the theoretical models do not differentiate between RRab and RRC stars, in Fig. 5 we show the *i* band PLZ relation derived for the mixed population in this work with the parallax method and recalculated onto the SDSS photometric system according to the linear equations given in Table 6 of Tonry et al. (2012) for two constant metallicities $[\text{Fe}/\text{H}] = -0.5$ and -2.0 dex. With red, green and yellow lines we overplotted the relations given by Equation (10) for the same metallicity values and three different values of $[\alpha/\text{Fe}] = -0.1, +0.2$ and $+0.5$ dex, respectively. The disagreement between our result and relation from Cáceres & Catelan (2008) is significant. Firstly, the slope of -1.035 from Cáceres & Catelan (2008) is flatter than our -1.469 ± 0.328 . The relations are also shifted in the ZP relative to ours, and that shift is larger for lower metallicities. Finally, Fig. 5 shows that the change of the ZP strongly depends on the $[\alpha/\text{Fe}]$ value. For metallicity $[\text{Fe}/\text{H}] = -0.5$ dex at $\log P = -0.25$ days (equal to the pivot $\log P_0$), the ZP shift between our and the theoretical relation is about 0.18, 0.13 and 0.08 mag for $[\alpha/\text{Fe}] = -0.1, +0.2$ and $+0.5$ dex, respectively. The same values for $[\text{Fe}/\text{H}] = -2.0$ dex are 0.21, 0.16 and 0.11. The ZP shift for all four methods are given in Table B.1. The significant change of the ZP depending on the $[\alpha/\text{Fe}]$ value

might partially explain the differences between our relations for RR Lyr stars from the vicinity of the Sun and RR Lyr stars from the globular clusters, presented in the next Section 4.3.2, as the $[\alpha/\text{Fe}]$ ratio is different for RR Lyr stars in different environments (see for example Figure 4 in Pritzl et al. 2005). Also, our sample of stars is far more heterogeneous in terms of $[\alpha/\text{Fe}]$ ratio than a typical globular cluster.

Marconi et al. (2022) published theoretical PLZ relations for RR Lyr stars in the Rubin-LSST filter system, using theoretical bolometric corrections based on the expected performance throughput curves for the Rubin-LSST photometric system. In absence of transformation equations between the (observed) Rubin-LSST bands and the PS1 system, comparing their relations to our result would be a nontrivial task, so we decided not to perform it.

4.3.2. Comparison with empirical PLZ relations

Sesar et al. (2017) derived empirical PLZ relations based on 55 RRab stars located in five globular clusters with magnitudes in the *griz* Pan-STARSS1 bands. They used a probabilistic approach to constrain their relations. In Figure 6 we show the comparison of our original PLZ relations for RRab stars derived with parallax method, with overplotted relations from Sesar et al. (2017) given with their Equation 4, where the coefficient values were taken from their Table 1. The comparison is made for two constant metallicities ($[\text{Fe}/\text{H}] = -0.5$ and -2.0 dex). The first evident disagreement between our result and Sesar et al. (2017) are the slopes of the relations. Both the dependences of the period and metallicity in Sesar et al. (2017) are roughly constant in all three Sloan $g_{P1}r_{P1}i_{P1}$ bands, while in our case they change depending on the filter. The slopes of the period dependence in Sesar et al. (2017) are steep (of about -1.7), while our g_{P1} band PLZ relation is almost flat (-0.527), then becoming steeper at about -1.47 in the i_{P1} band. Also, the metallicity slopes in Sesar et al. (2017) are close to zero in all three bands while our slopes are between about $0.2 - 0.3$ mag/dex and flatten toward longer wavelengths. Sesar et al. (2017) used the stars from a much narrower metallicity range than we (from -1.02 to -2.37 dex versus from -0.03 to -2.59 dex) which might partially explain their very small dependence on the metallicity. The shift in the ZP between compared relations is quite large for higher metallicities. For $[\text{Fe}/\text{H}] = -0.5$ dex and $\log P = -0.25$ days it is about 0.2 in all three filters while for $[\text{Fe}/\text{H}] = -2.0$ dex it is about $-0.04, 0.04$ and 0.08 for $g_{P1}r_{P1}i_{P1}$ bands, respectively. The values of the ZP shifts calculated for all four methods are presented in Table B.2.

Vivas et al. (2017) provided empirical PLZ relations for the RR Lyr stars from the globular cluster M5. Their data for 47 RRab and 14 RRC stars were gathered with DECam and *ugriz* filters. In Figure 7 we present the comparison of our original $g_{P1}r_{P1}i_{P1}$ band PLZ relations for RRab stars derived with the parallax method for a constant metallicity $[\text{Fe}/\text{H}] = -1.25$ dex, as adopted by Vivas et al. (2017) for M5, with overplotted relations recalculated onto the Pan-STARSS photometric system using the calibration equations for a Dark Energy Survey (DES) photometric system from Appendix B of Abbott et al. (2021). Red lines show the dereddened and scaled relations given by Equation (3) in Vivas et al. (2017) for the DM of 14.44 mag (± 0.02 mag) adopted by them, while the magenta line show the relations from Table 8 shifted by DM = 14.37 mag (± 0.02 mag) taken from Table 1 of Baumgardt & Vasiliev (2021). The slopes of our relations and Vivas et al. (2017) are in a good agreement with each other, and agree within 1σ uncertainties. The

ZP, however, is quite different. For a $\log P = -0.25$ days and $DM = 14.44$ mag the shift in the ZP is about 0.33, 0.25 and 0.23 mag for $g_{P1}r_{P1}i_{P1}$ filters, respectively. Using the alternative value of DM would change those shifts to about 0.26, 0.18 and 0.17 mag. This comparison shows that the choice of the DM value used for putting the ZP of a globular cluster to an absolute scale is critical. In this work we used Gaia DR3 parallaxes for the calculation of the distance to our stars, which is the most direct and precise method known today.

Bhardwaj et al. (2021) presented a study of the PL relations of RR Lyr stars in the globular cluster M15 in SDSS gi bands. To compare their results with ours, we recalculated our PLZ relations for RRab stars and mixed population obtained with parallax method onto the SDSS system (Tonry et al. 2012). The slope values for both relations agree well within 1σ uncertainties. However, the difference of the ZP is, again, significant. The shift of the ZP calculated for a constant metallicity $[Fe/H] = -2.33$ dex and $DM = 15.15$ mag (± 0.02 mag) adopted by Bhardwaj et al. (2021) for M15 at $\log P = -0.25$ days is about 0.17 and 0.21 mag for RRab stars, and 0.18 and 0.20 mag for RRab+RRc stars for SDSS gi bands, respectively.

Ngeow et al. (2022) derived their PL relations for the gri Pan-STARSS magnitudes as well as Wesenheit indices defined in an identical way as the ones used in this work (see Section 2.3) for RRab, RRc and RRab+RRc stars located in 46 globular clusters. In Figure 8 we show the comparison of our original PLZ relations for $g_{P1}r_{P1}i_{P1}$ magnitudes and Wesenheit indices of RRab stars derived with the parallax method. Overplotted with red lines are relations from Ngeow et al. (2022) given with Equation (1) and coefficients from their Table 4 for two constant metallicities $[Fe/H] = -0.5$ and -2.0 dex. Once again, the slopes of the period dependence agree well within 1σ uncertainties between both results, while our slopes are systematically steeper than those of Ngeow et al. (2022). The agreement of the metallicity slope is slightly worse, as the slopes agree within 2σ . One of the possible reasons of this could be that Ngeow et al. (2022) use a narrower range of metallicities (from -0.43 to -2.36 dex versus our from -0.03 to -2.59 dex). The difference of the ZP in case of the $g_{P1}r_{P1}i_{P1}$ magnitudes is significant. The shift of the ZP for RRab stars at the $\log P = -0.25$ days for $[Fe/H] = -0.5$ dex is about 0.41 mag for the g_{P1} band and 0.32, 0.28 mag in the $r_{P1}i_{P1}$ bands, respectively. The same shifts for $[Fe/H] = -2.0$ dex are smaller (0.26, 0.22 and 0.24 mag). A better agreement we see, however, for the Wesenheit magnitudes, where the shift for $[Fe/H] = -0.5$ dex at the $\log P = -0.25$ days for RRab stars is about 0.02 and 0.04 mag for W_r^{ri} and W_g^{gi} , and slightly larger for W_g^{gr} (≈ 0.11 mag). Those values grow for $[Fe/H] = -2.0$ dex and are, respectively, about 0.19, 0.16 mag and 0.15 mag.

The slopes of the period dependence of the PLZ relations derived in this work are in a quite good agreement with other studies in the globular clusters (especially Vivas et al. 2017; Bhardwaj et al. 2021; Ngeow et al. 2022). Larger differences occur for the metallicity slopes, which might be due to the use of different metallicity ranges. In case of the globular clusters this is generally much narrower (e.g., Sesar et al. 2017; Ngeow et al. 2022). The largest differences, however, we see in the ZPs of the relations. Our ZPs are systematically fainter than all other studies. There might be several potential reasons for this state of affairs. For example, as we can see in Figure 5, the value of $[\alpha/Fe]$ ratio might influence noticeably the ZP of the PLZ relation, which might be another factor differentiating the results in globular clusters and those from the vicinity of the Sun. The

metallicity slope uncertainty also influences the ZP of the relation, so the more stars from larger metallicity range are used, the better. Even though we can boast a wide range of metallicities, the number of stars used for our fitting is rather small. An additional difficulty might be the fact that metallicities are on different metallicity scales. The knowledge of the accurate distances of stars is crucial in determination of the absolute PL and PLZ relations, which still is a problem in case of globular clusters (as we can see for example in Figure 7). The sample of RR Lyr stars used in the current study is located less than 3 kpc around the Sun, so the good quality Gaia DR3 parallaxes were available for them. Also, calculation of the reddening for the stars was performed differently in different studies (e.g., Vivas et al. 2017; Bhardwaj et al. 2021). Last but not least, the fact that our relations seem to be shifted systematically relative to globular clusters suggests a possible problem of blending of those stars with much fainter background or foreground stars in the globular clusters which, in a consequence, might slightly change their apparent magnitudes. For the discussion of the influence of the blending see, for instance, the study of Majaess et al. (2012). This problem does not appear to exist in our data.

4.4. Revision of the photometric correctness

The significant discrepancy between the ZPs determined by us and those in the literature motivated us to analyze the spectral energy distribution (SED) for some of our stars, in order to check the correctness of the mean magnitudes of RR Lyr stars in the Sloan–Pan-STARSS bands. We used Virtual Observatory Spectral Energy Distribution Analyzer (VOSA, Bayo et al. 2008) to compare the SED of 18 RR Lyr stars common with the sample of stars from Monson et al. (2017), where they compiled in their Table 5 mean magnitudes of RR Lyr stars in the $UBVR_CI_CJHK_sW_1W_2$ bands. Our mean apparent magnitudes matched very well the ones from Monson et al. (2017) on the SED, except for V675 Sgr, where our photometry in the Sloan–Pan-STARSS $g_{P1}r_{P1}i_{P1}$ bands is systematically fainter (by about 0.1 mag). The reason for that is unclear. V675 Sgr is located in a dense field toward the Galactic Bulge, which may affect aperture photometry. Another possibility is that the ATLAS-REFCAT2 itself might have a systematic bias in the magnitudes of stars in this area. We marked this problematic star in Table 1 with a star-symbol, and we recommend using the mean magnitudes given for it with caution. Nevertheless, this one problematic star is not influencing the overall result much, and consequently, do not explain the obtained discrepancy in the ZP between this work and the literature.

5. Summary

In this work, we have derived PL and PLZ relations in the $g_{P1}r_{P1}i_{P1}$ Sloan–Pan-STARSS bands, together with their Wesenheit index counterparts (W_r^{ri} , W_r^{gr} , and W_g^{gi}) for Galactic RR Lyr stars located within a radius of about 3 kpc around the Sun. Data for the project were acquired with the 40 cm LCO Telescope Network in the $g'r'i'$ Sloan filters, and calibrated using the ATLAS-REFCAT2 (Tonry et al. 2018) catalog, which is on the Pan-STARSS implementation of the Sloan photometric system. Well covered light curves for 44 RRab and nine RRc type stars are presented in Figures A.1 and A.2, respectively, in the Appendix A. The mean magnitudes obtained based on the resulting light curves are given in Table 1. The adopted reddening values from Schlafly & Finkbeiner (2011) were available for all our

stars, and the extinction coefficients were taken from Green et al. (2019). The PL and PW relations were derived using 38 RRab and seven RRc stars, separately, as well as for a mixed population of RRab+RRc stars (45 stars in total). The PLZ and PWZ relations were derived based on 31 RRab stars and 35 stars in total for the mixed population, as not all stars in the original sample had metallicity values available in Crestani et al. (2021b,a). The relations were determined using absolute magnitudes calculated in four ways: directly from geometric Gaia DR3 parallaxes, the ABL method, and using geometric and photogeometric distances from Bailer-Jones et al. (2021). The resulting coefficients are given in Tables 2 and 3.

We noticed that the fundamentalization procedure of the RRc stars from Iben (1974) failed to align the RRc and RRab stars correctly, and instead introduced the systematic shift seen in Figures 2 and 3, which depends on the filter used. We discussed different approaches to the fundamentalization procedure of the RRc stars, first by following the method of Zgirski et al. (2023), and then the nonlinear relation showed in Nemec et al. (2024). None of the proposed approaches fully removes the existing offset, as it is a manifestation of the temperature (and hence color) difference propagating into the PL and PLZ relations. For this reason, for distance determination purposes we recommend to use the relations derived separately for RRab and RRc stars.

We tested the behavior of our PL, PW, PLZ and PWZ relations in case of applying parallax corrections from Groenewegen (2021) or not applying them at all. In the first case, the differences in slopes and ZPs of the original and new relations are statistically insignificant. In the second case, the new intercepts were noticeably smaller. This exercise shows that uncertainties related to the ZP of Gaia parallaxes are significant.

The comparison of the PLZ and PWZ relations presented in this work with available literature studies showed that our slopes of the period dependence are in a good agreement with some of the works (e.g., Vivas et al. 2017; Bhardwaj et al. 2021; Ngeow et al. 2022), becoming steeper for longer wavelengths, but do they not agree with theoretical study of Cáceres & Catelan (2008) or the empirical PL relations from Sesar et al. (2017). The metallicity slopes obtained in this work are steeper than other literature values, and the reason for that might be, that the metallicity range we use is larger than the metallicity range of globular clusters studied by other authors. The ZPs obtained in this work are systematically fainter than the literature ZPs, however, this conclusion should be treated with caution because the comparison of our and literature results is not straightforward due to the number of reasons. We are comparing different populations of stars which might differ according to, for example, $[\alpha/\text{Fe}]$ content which is influencing the ZP of the PLZ relation (as shown in Figure 5). Also, the metallicity slope have an influence on the ZP, and that slope is steeper in our case. Our results are also not based on many stars, although, as the study of the SED showed, our photometry is of very good quality, and we also use good quality Gaia DR3 parallaxes, which further assures us about the correctness of procedures applied in this work.

Presented PL, PW, PLZ and PWZ relations in the Sloan-Pan-STARSS bands, to the best of our knowledge, are the first of their kind for RR Lyr stars from the vicinity of the Sun. So we hope that as such they will be useful for distance determinations of RR Lyr stars in the upcoming Rubin-LSST era.

Acknowledgements. We thank the anonymous referee for valuable comments to the content of the paper. We thank prof. Pawel Moskalik for valuable discussion about the RRd stars. The research leading to these results has received funding from the European Research Council (ERC) under the European Union's Horizon 2020 research and innovation program (grant agreement

No. 695099). We also acknowledge support from the National Science Center, Poland grants MAESTRO UMO-2017/26/A/ST9/00446, BEETHOVEN UMO-2018/31/G/ST9/03050 and DIR/WK/2018/09 grants of the Polish Ministry of Science and Higher Education. We also acknowledge financial support from Uni-versScale grant financed by the European Union's Horizon 2020 research and innovation programme under the grant agreement number 951549. We gratefully acknowledge financial support for this work from the BASAL Centro de Astrofísica y Tecnologías Afines (CATA) AFB-170002 and the Millenium Institute of Astrophysics (MAS) of the Iniciativa Científica Milenio del Ministerio de Economía, Fomento y Turismo de Chile, project IC120009. W.G. also gratefully acknowledges support from the ANID BASAL project ACE210002. P.W. gratefully acknowledges financial support from the Polish National Science Center grant PRELUDIUM 2018/31/N/ST9/02742. This work has made use of data from the European Space Agency (ESA) mission Gaia (<https://www.cosmos.esa.int/gaia>), processed by the Gaia Data Processing and Analysis Consortium (DPAC, <https://www.cosmos.esa.int/web/gaia/dpac/consortium>). Funding for the DPAC has been provided by national institutions, in particular the institutions participating in the Gaia Multilateral Agreement. This publication makes use of VOSA, developed under the Spanish Virtual Observatory (<https://svo.cab.inta-csic.es>) project funded by MCIN/AEI/10.13039/501100011033/ through grant PID2020-112949GB-I00. VOSA has been partially updated by using funding from the European Union's Horizon 2020 Research and Innovation Programme, under Grant Agreement n 776403 (EXOPLANETS-A). Facilities: LCOGT (0.4m). Software used in this work: gaiadr3_zero-point (Lindgren et al. 2021), IRAF (Tody 1986, 1993), DAOPHOT (Stetson 1987), Astropy (Astropy Collaboration et al. 2013), Sklearn (Pedregosa et al. 2011) NumPy (van der Walt et al. 2011; Harris et al. 2020), SciPy (Virtanen et al. 2020), Matplotlib (Hunter 2007), VOSA (Bayo et al. 2008).

References

- Abazajian, K., Adelman-McCarthy, J. K., Agüeros, M. A., et al. 2003, *AJ*, 126, 2081
- Abbott, T. M. C., Adamów, M., Aguena, M., et al. 2021, *ApJS*, 255, 20
- Arenou, F. & Luri, X. 1999, in *Astronomical Society of the Pacific Conference Series*, Vol. 167, *Harmonizing Cosmic Distance Scales in a Post-HIPPARCOS Era*, ed. D. Egret & A. Heck, 13–32
- Astropy Collaboration, Robitaille, T. P., Tollerud, E. J., et al. 2013, *A&A*, 558, A33
- Bailer-Jones, C. A. L., Rybizki, J., Fousneau, M., Demleitner, M., & Andrae, R. 2021, *AJ*, 161, 147
- Bailey, S. I. 1902, *Annals of Harvard College Observatory*, 38, 1
- Bailey, S. I. & Pickering, E. C. 1913, *Annals of Harvard College Observatory*, 78, 1
- Baumgardt, H. & Vasiliev, E. 2021, *MNRAS*, 505, 5957
- Bayo, A., Rodrigo, C., Barrado Y Navascués, D., et al. 2008, *A&A*, 492, 277
- Bellm, E. C., Kulkarni, S. R., Barlow, T., et al. 2019, *PASP*, 131, 068003
- Bellm, E. C., Kulkarni, S. R., Graham, M. J., et al. 2018, *Publications of the Astronomical Society of the Pacific*, 131, 018002
- Bhardwaj, A. 2024, *IAU Symposium*, 376, 250
- Bhardwaj, A., Marconi, M., Rejkuba, M., et al. 2023, *ApJ*, 944, L51
- Bhardwaj, A., Rejkuba, M., Sloan, G. C., Marconi, M., & Yang, S.-C. 2021, *ApJ*, 922, 20
- Braga, V. F., Stetson, P. B., Bono, G., et al. 2018, *AJ*, 155, 137
- Breuval, L., Kervella, P., Wielgórski, P., et al. 2021, *The Astrophysical Journal*, 913, 38
- Cáceres, C. & Catelan, M. 2008, *ApJS*, 179, 242
- Catelan, M. 2009, *Ap&SS*, 320, 261
- Crestani, J., Braga, V. F., Fabrizio, M., et al. 2021a, *ApJ*, 914, 10
- Crestani, J., Fabrizio, M., Braga, V. F., et al. 2021b, *ApJ*, 908, 20
- Dekany, R., Smith, R. M., Riddle, R., et al. 2020, *Publications of the Astronomical Society of the Pacific*, 132, 038001
- Demers, S. & Wehlau, A. 1977, *AJ*, 82, 620
- Drimmel, R. & Spergel, D. N. 2001, *ApJ*, 556, 181
- Feast, M. W. & Catchpole, R. M. 1997, *MNRAS*, 286, L1
- Flaugher, B., Diehl, H. T., Honscheid, K., et al. 2015, *AJ*, 150, 150
- Fukugita, M., Ichikawa, T., Gunn, J. E., et al. 1996, *AJ*, 111, 1748
- Gaia Collaboration, Vallenari, A., Brown, A. G. A., et al. 2023, *A&A*, 674, A1
- Green, G. M., Schlafly, E., Zucker, C., Speagle, J. S., & Finkbeiner, D. 2019, *ApJ*, 887, 93
- Groenewegen, M. A. T. 2021, *A&A*, 654, A20
- Harris, C. R., Millman, K. J., van der Walt, S. J., et al. 2020, *Nature*, 585, 357
- Hunter, J. D. 2007, *Computing in Science and Engineering*, 9, 90
- Iben, I. J. 1974, *ARA&A*, 12, 215
- Iben, I. J. & Huchra, J. 1971, *A&A*, 14, 293
- Ivezić, Ž., Kahn, S. M., Tyson, J. A., et al. 2019, *ApJ*, 873, 111

Table 1. MW RR Lyr star sample and their main parameters.

Star	Period (days)	ϖ_{DR3} (mas)	RUWE	GOF (mag)	E(B-V)	$\langle g \rangle$ (mag)	$\langle r \rangle$ (mag)	$\langle i \rangle$ (mag)	[Fe/H] (dex)	Source
RRab										
AA Aql	0.3617877	0.7615 ± 0.0179	1.14	3.96	0.0710 ± 0.0059	11.907 ± 0.004	11.786 ± 0.003	11.780 ± 0.003	-0.42 ± 0.11	1
AV Peg	0.3903814	1.5075 ± 0.0176	1.25	5.44	0.0520 ± 0.0007	10.606 ± 0.003	10.417 ± 0.002	10.395 ± 0.002	-0.03 ± 0.07	1
BB Eri ^a	0.5699697	0.7216 ± 0.0238	1.74	22.82	0.0430 ± 0.0015	11.628 ± 0.003	11.447 ± 0.003	11.392 ± 0.003	-1.66 ± 0.07	1
BH Peg	0.640993	1.1813 ± 0.0226	1.22	3.97	0.0700 ± 0.0008	10.629 ± 0.008	10.346 ± 0.005	10.247 ± 0.005	-	-
BK Tuc	0.5500676	0.3630 ± 0.0172	1.34	8.98	0.0240 ± 0.0004	12.906 ± 0.007	12.741 ± 0.006	12.715 ± 0.006	-1.86 ± 0.01	1
BR Aqr	0.4818717	0.8075 ± 0.0217	0.90	-2.09	0.0240 ± 0.0002	11.525 ± 0.002	11.367 ± 0.003	11.333 ± 0.005	-0.94 ± 0.07	1
BT Aqr ^a	0.4063595	0.5365 ± 0.0220	1.41	12.11	0.0400 ± 0.0002	12.502 ± 0.003	12.343 ± 0.002	12.322 ± 0.003	-0.24 ± 0.04	1
CD Vel	0.5735076	0.5874 ± 0.0137	1.26	7.44	0.1920 ± 0.0055	12.185 ± 0.006	11.953 ± 0.005	11.862 ± 0.004	-1.84 ± 0.09	1
CP Aqr	0.4634018	0.7754 ± 0.0236	1.04	0.78	0.0500 ± 0.0016	11.883 ± 0.007	11.755 ± 0.004	11.740 ± 0.003	-0.62 ± 0.04	1
DH Hyat ^a	0.4890007	0.5033 ± 0.0266	1.55	16.42	0.0370 ± 0.0031	12.263 ± 0.003	12.147 ± 0.003	12.125 ± 0.003	-1.78 ± 0.04	1
DN Aqr	0.6337558	0.7785 ± 0.0195	0.95	-0.97	0.0220 ± 0.0007	11.336 ± 0.006	11.170 ± 0.004	11.111 ± 0.006	-1.74 ± 0.03	1
DX Del	0.4726191	1.7584 ± 0.0150	0.99	-0.43	0.0800 ± 0.0018	10.096 ± 0.002	9.859 ± 0.002	9.792 ± 0.003	-0.43 ± 0.08	1
EW Cam	0.628408	1.7499 ± 0.0136	1.04	1.30	0.0180 ± 0.0007	9.706 ± 0.003	9.492 ± 0.002	9.394 ± 0.002	-	-
HH Pup	0.3907454	1.1377 ± 0.0151	1.07	1.82	0.1240 ± 0.0054	11.408 ± 0.005	11.195 ± 0.004	11.123 ± 0.003	-0.73 ± 0.02	1
RR Cet	0.55302836	1.6217 ± 0.0213	1.01	0.43	0.0200 ± 0.0003	9.835 ± 0.006	9.681 ± 0.007	9.640 ± 0.006	-1.63 ± 0.10	1
RR Leo	0.4524021	1.0836 ± 0.0248	1.12	2.75	0.0340 ± 0.0035	10.816 ± 0.003	10.720 ± 0.002	10.721 ± 0.001	-0.47 ± 0.04	1
RU Scl	0.4933549	1.2800 ± 0.0317	1.24	5.20	0.0170 ± 0.0004	10.308 ± 0.008	10.207 ± 0.005	10.201 ± 0.004	-1.58 ± 0.08	1
RY Cet	0.62341	0.9762 ± 0.0177	1.14	3.21	0.0270 ± 0.0006	11.059 ± 0.005	10.844 ± 0.004	10.776 ± 0.004	-1.45 ± 0.06	1
RV Phe ^a	0.5964071	0.5606 ± 0.0197	1.44	14.27	0.0070 ± 0.0005	12.039 ± 0.003	11.856 ± 0.003	11.801 ± 0.004	-1.50 ± 0.03	1
RX Cet	0.57373	0.7647 ± 0.0303	1.33	6.21	0.0240 ± 0.0007	11.526 ± 0.006	11.346 ± 0.005	11.307 ± 0.004	-1.53 ± 0.04	1
RX Eri	0.5872453	1.7229 ± 0.0225	1.28	8.44	0.0530 ± 0.0018	9.810 ± 0.003	9.593 ± 0.003	9.548 ± 0.003	-1.51 ± 0.08	1
S Ara	0.451848	1.1271 ± 0.0169	1.04	0.94	0.0880 ± 0.0027	10.839 ± 0.015	10.707 ± 0.010	10.679 ± 0.009	-1.40 ± 0.04	1
SS For	0.49543	1.2868 ± 0.0205	1.27	8.44	0.0130 ± 0.0002	10.465 ± 0.024	10.297 ± 0.019	10.269 ± 0.010	-	-
ST Pic	0.4857445	2.0822 ± 0.0123	1.00	-0.03	0.0270 ± 0.0012	9.568 ± 0.002	9.459 ± 0.002	9.433 ± 0.002	-	-
SV Eri	0.713877	1.3609 ± 0.0236	0.98	-0.40	0.0780 ± 0.0023	10.122 ± 0.005	9.892 ± 0.004	9.798 ± 0.002	-2.22 ± 0.03	1
SW And	0.442262	1.9954 ± 0.0284	1.20	5.23	0.0330 ± 0.0011	9.812 ± 0.003	9.603 ± 0.004	9.567 ± 0.004	-0.17 ± 0.05	2
SX For	0.6053423	0.8680 ± 0.0146	0.97	-0.99	0.0120 ± 0.0009	11.245 ± 0.003	11.051 ± 0.003	11.000 ± 0.003	-1.81 ± 0.01	1
SZ Gem ^a	0.5011303	0.7004 ± 0.0248	1.44	10.70	0.0380 ± 0.0004	11.822 ± 0.002	11.715 ± 0.002	11.697 ± 0.002	-1.87 ± 0.10	2
TU Lyn	0.597434355	1.4798 ± 0.0160	0.86	-3.57	0.0150 ± 0.0005	10.019 ± 0.006	9.806 ± 0.005	9.746 ± 0.003	-1.53 ± 0.01	2
U Lep	0.5814789	0.9889 ± 0.0167	1.33	9.72	0.0290 ± 0.0015	10.671 ± 0.005	10.553 ± 0.003	10.534 ± 0.004	-1.88 ± 0.28	1
U Pic	0.4403750	0.8236 ± 0.0128	0.92	4.83	0.0090 ± 0.0002	11.465 ± 0.004	11.342 ± 0.004	11.345 ± 0.004	-0.82 ± 0.03	1
UU Cet	0.6060736	0.5334 ± 0.0191	1.20	2.09	0.0200 ± 0.0006	12.174 ± 0.004	11.972 ± 0.004	11.919 ± 0.004	-1.66 ± 0.04	2
V341 Aql	0.5780230	0.8822 ± 0.0230	1.21	5.61	0.0790 ± 0.0021	10.955 ± 0.003	10.827 ± 0.003	10.808 ± 0.003	-1.47 ± 0.04	1
V4424 Sgr	0.4245034	1.7868 ± 0.0145	1.05	1.22	0.0890 ± 0.0029	10.496 ± 0.006	10.179 ± 0.003	10.140 ± 0.003	-	-
V675 Sgr ^a	0.6422935	1.1993 ± 0.0188	0.75	-5.51	0.0910 ± 0.0055	10.536 ± 0.002	10.337 ± 0.002	10.279 ± 0.003	-2.47 ± 0.02	2
V Ind	0.4796017	1.5058 ± 0.0191	1.00	0.02	0.0400 ± 0.0009	10.076 ± 0.005	9.963 ± 0.002	9.985 ± 0.003	-1.63 ± 0.03	1
VW Scl ^a	0.5109117	0.9027 ± 0.0338	1.74	26.98	0.0140 ± 0.0011	11.106 ± 0.005	11.016 ± 0.004	11.043 ± 0.004	-1.38 ± 0.23	1
W Tuc	0.6422382	0.6276 ± 0.0133	0.98	-0.58	0.0180 ± 0.0002	11.504 ± 0.003	11.393 ± 0.003	11.371 ± 0.003	-1.90 ± 0.08	1
WY Ant	0.5743427	0.9787 ± 0.0208	1.11	3.29	0.0550 ± 0.0009	10.995 ± 0.005	10.803 ± 0.004	10.744 ± 0.004	-1.95 ± 0.06	1
X Ari	0.6511796	1.8690 ± 0.0188	1.22	4.48	0.1670 ± 0.0053	9.798 ± 0.026	9.452 ± 0.006	9.323 ± 0.008	-2.59 ± 0.05	1
X Ret	0.49201	0.6590 ± 0.0144	1.38	9.78	0.0400 ± 0.0022	11.809 ± 0.009	11.663 ± 0.007	11.647 ± 0.006	-	-
XZ Gru	0.8831035	0.8700 ± 0.0185	1.12	2.76	0.0040 ± 0.0006	10.864 ± 0.004	10.647 ± 0.004	10.575 ± 0.004	-	-
Z Mic	0.5869258	0.8190 ± 0.0230	0.96	-0.83	0.0820 ± 0.0028	11.792 ± 0.003	11.507 ± 0.003	11.397 ± 0.002	-1.58 ± 0.05	1
RRc										
AE Boo	0.3148921	1.1432 ± 0.0190	1.06	1.45	0.0230 ± 0.0012	10.722 ± 0.004	10.662 ± 0.003	10.681 ± 0.002	-1.62 ± 0.09	1
CS Eri	0.311331	2.1665 ± 0.0158	1.05	1.38	0.0170 ± 0.0004	9.056 ± 0.006	9.052 ± 0.006	9.050 ± 0.007	-1.97 ± 0.09	1
EV Psc	0.3062573	1.1328 ± 0.0300	1.12	3.21	0.0300 ± 0.0008	10.640 ± 0.003	10.555 ± 0.003	10.575 ± 0.003	-	-
IY Eri	0.375026	0.7626 ± 0.0133	0.96	-1.10	0.0230 ± 0.0011	11.133 ± 0.005	11.067 ± 0.004	11.109 ± 0.003	-	-
LS Her	0.230808	1.0254 ± 0.0206	0.98	-0.36	0.0360 ± 0.0009	10.977 ± 0.009	10.957 ± 0.007	11.006 ± 0.005	-	-
MT Tel ^a	0.3169011	2.0704 ± 0.0301	1.65	11.93	0.0340 ± 0.0026	9.102 ± 0.006	9.085 ± 0.007	9.079 ± 0.004	-2.60 ± 0.18	1
RU Psc ^a	0.390385	1.2783 ± 0.0291	1.53	1.25	0.0390 ± 0.0002	10.333 ± 0.010	10.171 ± 0.006	10.157 ± 0.005	-	-
RU Sex	0.350232	0.9155 ± 0.0206	1.33	8.54	0.0270 ± 0.0006	10.885 ± 0.003	10.806 ± 0.002	10.821 ± 0.010	-1.97 ± 0.10	1
T Sex	0.32469759	1.3400 ± 0.0225	1.16	3.16	0.0420 ± 0.0032	10.124 ± 0.004	10.075 ± 0.003	10.090 ± 0.002	-1.49 ± 0.10	2

Star: name of a RR Lyr star; Period: period of a RR Lyr star adopted from AAVSO database; ϖ_{DR3} : parallax from the Gaia DR3 catalog corrected with RUWE; renormalized unit weight error from the Gaia DR3 catalog; GOF: goodness-of-fit from the Gaia DR3 catalog; E(B-V): reddening value adopted from Schlafly & Finkbeiner (2011) reddening map corrected for the MW model by Drimmel & Spiegel (2001); $\langle g \rangle$, $\langle r \rangle$, $\langle i \rangle$: intensity-averaged mean magnitude from Fourier series fitting for the Pan-STARRS $g_{r1}r_{11}i_{11}$ filters, respectively; [Fe/H]: the adopted iron abundance; Source: source of iron abundance (1 - Crestani et al. 2021b; 2 - Crestani et al. 2021a).

^a Stars rejected based on the RUWE and GOF parallax quality parameters, given by the Gaia DR3 catalog.

^{*} The SED showed that the Sloan g_{r1} mean magnitudes are systematically fainter than the photometric compilation from Monson et al. (2017).

Table 2. Determined PL and PW relations for Galactic RR Lyr stars of type RRab and RRc, as well as for the combined population.

band	type	(parallax):				(geometric distances):			
		a_λ	b_λ	rms	N	a_λ	b_λ	rms	N
<i>g</i>	RRab	-2.242 ± 0.376	0.805 ± 0.031	0.18	38	-2.162 ± 0.382	0.802 ± 0.031	0.18	38
	RRc	-1.984 ± 0.760	0.605 ± 0.062	0.11	7	-1.983 ± 0.746	0.604 ± 0.061	0.11	7
	RRab+RRc	-1.500 ± 0.368	0.773 ± 0.034	0.21	45	-1.448 ± 0.368	0.771 ± 0.034	0.21	45
<i>r</i>	RRab	-2.528 ± 0.300	0.660 ± 0.025	0.14	38	-2.447 ± 0.308	0.657 ± 0.025	0.15	38
	RRc	-2.266 ± 0.705	0.557 ± 0.058	0.10	7	-2.266 ± 0.694	0.556 ± 0.057	0.10	7
	RRab+RRc	-1.929 ± 0.296	0.634 ± 0.028	0.17	45	-1.878 ± 0.297	0.633 ± 0.028	0.17	45
<i>i</i>	RRab	-2.799 ± 0.296	0.642 ± 0.022	0.13	38	-2.718 ± 0.278	0.639 ± 0.023	0.13	38
	RRc	-2.393 ± 0.647	0.598 ± 0.053	0.10	7	-2.392 ± 0.637	0.597 ± 0.052	0.09	7
	RRab+RRc	-2.249 ± 0.266	0.619 ± 0.025	0.15	45	-2.197 ± 0.267	0.618 ± 0.025	0.15	45
W_r^{ri}	RRab	-3.626 ± 0.218	0.587 ± 0.018	0.11	38	-3.546 ± 0.229	0.584 ± 0.019	0.11	38
	RRc	-2.780 ± 0.515	0.723 ± 0.042	0.08	7	-2.779 ± 0.508	0.722 ± 0.042	0.08	7
	RRab+RRc	-3.226 ± 0.202	0.574 ± 0.019	0.12	45	-3.174 ± 0.206	0.572 ± 0.019	0.12	45
W_r^{gr}	RRab	-3.357 ± 0.231	0.239 ± 0.019	0.11	38	-3.277 ± 0.237	0.237 ± 0.019	0.11	38
	RRc	-3.086 ± 0.643	0.415 ± 0.053	0.10	7	-3.085 ± 0.644	0.414 ± 0.053	0.10	7
	RRab+RRc	-3.175 ± 0.195	0.232 ± 0.018	0.11	45	-3.123 ± 0.198	0.231 ± 0.018	0.11	45
W_g^{gi}	RRab	-3.508 ± 0.202	0.434 ± 0.016	0.10	38	-3.427 ± 0.211	0.432 ± 0.017	0.10	38
	RRc	-2.914 ± 0.545	0.588 ± 0.045	0.08	7	-2.913 ± 0.542	0.587 ± 0.044	0.08	7
	RRab+RRc	-3.157 ± 0.182	0.424 ± 0.015	0.09	45	-3.151 ± 0.185	0.423 ± 0.017	0.11	45
		(ABL method):				(photo-geometric distances):			
<i>g</i>	RRab	-2.318 ± 0.373	0.810 ± 0.032	0.18	38	-2.179 ± 0.382	0.803 ± 0.031	0.18	38
	RRc	-1.862 ± 0.737	0.615 ± 0.066	0.11	7	-2.035 ± 0.743	0.607 ± 0.061	0.11	7
	RRab+RRc	-1.506 ± 0.372	0.783 ± 0.037	0.21	45	-1.462 ± 0.367	0.771 ± 0.034	0.21	45
<i>r</i>	RRab	-2.594 ± 0.297	0.663 ± 0.026	0.14	38	-2.465 ± 0.309	0.658 ± 0.025	0.15	38
	RRc	-2.143 ± 0.679	0.566 ± 0.061	0.10	7	-2.317 ± 0.693	0.558 ± 0.057	0.10	7
	RRab+RRc	-1.918 ± 0.300	0.641 ± 0.030	0.17	45	-1.891 ± 0.296	0.633 ± 0.028	0.17	45
<i>i</i>	RRab	-2.870 ± 0.269	0.644 ± 0.023	0.13	38	-2.736 ± 0.279	0.640 ± 0.023	0.13	38
	RRc	-2.280 ± 0.621	0.606 ± 0.056	0.10	7	-2.444 ± 0.634	0.599 ± 0.052	0.09	7
	RRab+RRc	-2.230 ± 0.272	0.626 ± 0.027	0.15	45	-2.211 ± 0.265	0.618 ± 0.025	0.15	45
W_r^{ri}	RRab	-3.700 ± 0.227	0.587 ± 0.020	0.11	38	-3.563 ± 0.232	0.584 ± 0.019	0.11	38
	RRc	-2.707 ± 0.483	0.729 ± 0.045	0.08	7	-2.830 ± 0.500	0.725 ± 0.041	0.07	7
	RRab+RRc	-3.171 ± 0.215	0.580 ± 0.022	0.12	45	-3.185 ± 0.208	0.572 ± 0.019	0.12	45
W_r^{gr}	RRab	-3.395 ± 0.237	0.241 ± 0.021	0.11	38	-3.294 ± 0.243	0.237 ± 0.020	0.12	38
	RRc	-2.977 ± 0.602	0.423 ± 0.056	0.10	7	-3.137 ± 0.650	0.416 ± 0.053	0.10	7
	RRab+RRc	-3.146 ± 0.198	0.237 ± 0.021	0.11	45	-3.083 ± 0.182	0.225 ± 0.017	0.10	44
W_g^{gi}	RRab	-3.561 ± 0.205	0.435 ± 0.018	0.10	38	-3.445 ± 0.216	0.432 ± 0.018	0.10	38
	RRc	-2.827 ± 0.513	0.594 ± 0.048	0.08	7	-2.965 ± 0.540	0.590 ± 0.044	0.08	7
	RRab+RRc	-3.127 ± 0.166	0.422 ± 0.017	0.09	45	-3.114 ± 0.169	0.417 ± 0.016	0.10	44

Notes. band: the Pan-STARRS $g_{P1}r_{P1}i_{P1}$ bands and Wesenheit indicates constructed based on them using reddening vectors from Green et al. (2019); type: variability type of RR Lyr star; a_λ : slope of the fit; b_λ : zero point of the fit; rms: root mean square of derived relations; N: number of stars used for fitting. The logarithm of the pivot period used for fitting was $\log P_0 = -0.25$ for RRab and RRab+RRc stars, and $\log P_0 = -0.45$ for RRc type stars. Fundamentalization according to Iben (1974): $\log P_{ab} = \log P_c + 0.127$.

Jerzykiewicz, M. & Wenzel, W. 1977, *Acta Astron.*, 27, 35
Kaiser, N., Burgett, W., Chambers, K., et al. 2010, in *Society of Photo-Optical Instrumentation Engineers (SPIE) Conference Series*, Vol. 7733, *Ground-based and Airborne Telescopes III*, ed. L. M. Stepp, R. Gilmozzi, & H. J. Hall, 77330E
Kapteyn, J. C. 1890, *Astronomische Nachrichten*, 125, 165
Karczmarek, P., Pietrzyński, G., Gieren, W., et al. 2015, *AJ*, 150, 90
Karczmarek, P., Pietrzyński, G., Górski, M., Gieren, W., & Bersier, D. 2017, *AJ*, 154, 263
Kolláth, Z., Buchler, J. R., Szabó, R., & Csabry, Z. 2002, *A&A*, 385, 932
Lindegren, L., Bastian, U., Biermann, M., et al. 2021, *A&A*, 649, A4
Madore, B. F. 1982, *ApJ*, 253, 575
Majaess, D., Turner, D., Gieren, W., & Lane, D. 2012, *ApJ*, 752, L10
Marconi, M., Cignoni, M., Di Criscienzo, M., et al. 2006, *MNRAS*, 371, 1503
Marconi, M., Molinaro, R., Dall’Ora, M., et al. 2022, *ApJ*, 934, 29
Monson, A. J., Beaton, R. L., Scowcroft, V., et al. 2017, *AJ*, 153, 96
Narloch, W., Hajdu, G., Pietrzyński, G., et al. 2023, *ApJ*, 953, 14
Navarrete, C., Catelan, M., Contreras Ramos, R., et al. 2017, *A&A*, 604, A120
Nemec, J. M. 1985, *AJ*, 90, 204
Nemec, J. M., Linnell Nemec, A. F., Moskalik, P., et al. 2024, *MNRAS*, 529, 296

Ngeow, C.-C., Bhardwaj, A., Dekany, R., et al. 2022, *AJ*, 163, 239
Pedregosa, F., Varoquaux, G., Gramfort, A., et al. 2011, *Journal of Machine Learning Research*, 12, 2825
Pickering, E. C. 1901, *Astronomische Nachrichten*, 154, 423
Pietrzyński, G., Gieren, W., Szewczyk, O., et al. 2008, *AJ*, 135, 1993
Pritzl, B. J., Venn, K. A., & Irwin, M. 2005, *AJ*, 130, 2140
Riess, A. G., Casertano, S., Yuan, W., et al. 2021, *ApJ*, 908, L6
Sandage, A., Katem, B., & Sandage, M. 1981, *ApJS*, 46, 41
Schlafly, E. F. & Finkbeiner, D. P. 2011, *ApJ*, 737, 103
Sesar, B., Hernitschek, N., Mitrović, S., et al. 2017, *AJ*, 153, 204
Shapley, H. 1918, *PASP*, 30, 42
Stetson, P. B. 1987, *PASP*, 99, 191
Suchomska, K., Graczyk, D., Smolec, R., et al. 2015, *MNRAS*, 451, 651
Tody, D. 1986, in *Society of Photo-Optical Instrumentation Engineers (SPIE) Conference Series*, Vol. 627, *Instrumentation in astronomy VI*, ed. D. L. Crawford, 733
Tody, D. 1993, in *Astronomical Society of the Pacific Conference Series*, Vol. 52, *Astronomical Data Analysis Software and Systems II*, ed. R. J. Hanisch, R. J. V. Brissenden, & J. Barnes, 173
Tonry, J. L., Denneau, L., Flewelling, H., et al. 2018, *ApJ*, 867, 105

Table 3. Determined PLZ and PWZ relations for Galactic RR Lyr stars of type RRab and the RRab+RRc population using metallicities from Crestani et al. (2021b,a).

band	type	a_λ	b_λ	c_λ	rms	N
(parallax method):						
g	RRab	-0.527 ± 0.602	0.794 ± 0.028	0.264 ± 0.069	0.14	31
	RRab+RRc	-0.284 ± 0.439	0.791 ± 0.028	0.289 ± 0.053	0.14	35
r	RRab	-1.230 ± 0.493	0.651 ± 0.023	0.205 ± 0.056	0.12	31
	RRab+RRc	-1.017 ± 0.362	0.650 ± 0.023	0.228 ± 0.044	0.12	35
i	RRab	-1.682 ± 0.442	0.635 ± 0.021	0.174 ± 0.050	0.11	31
	RRab+RRc	-1.469 ± 0.328	0.633 ± 0.021	0.198 ± 0.040	0.11	35
W_r^{ri}	RRab	-3.061 ± 0.370	0.584 ± 0.017	0.082 ± 0.042	0.09	31
	RRab+RRc	-2.848 ± 0.275	0.583 ± 0.018	0.105 ± 0.033	0.09	35
W_r^{gr}	RRab	-3.273 ± 0.415	0.239 ± 0.020	0.033 ± 0.047	0.10	31
	RRab+RRc	-3.148 ± 0.305	0.238 ± 0.019	0.050 ± 0.037	0.10	35
W_g^{gi}	RRab	-3.154 ± 0.368	0.433 ± 0.017	0.060 ± 0.042	0.09	31
	RRab+RRc	-2.979 ± 0.271	0.432 ± 0.017	0.081 ± 0.033	0.09	35
(ABL method):						
g	RRab	-0.503 ± 0.550	0.798 ± 0.028	0.266 ± 0.063	0.14	31
	RRab+RRc	-0.290 ± 0.420	0.795 ± 0.028	0.290 ± 0.049	0.14	35
r	RRab	-1.227 ± 0.457	0.655 ± 0.023	0.204 ± 0.052	0.12	31
	RRab+RRc	-1.031 ± 0.349	0.652 ± 0.023	0.227 ± 0.041	0.12	35
i	RRab	-1.673 ± 0.413	0.638 ± 0.021	0.175 ± 0.047	0.11	31
	RRab+RRc	-1.479 ± 0.317	0.635 ± 0.022	0.197 ± 0.037	0.11	35
W_r^{ri}	RRab	-3.027 ± 0.362	0.587 ± 0.019	0.084 ± 0.042	0.09	31
	RRab+RRc	-2.837 ± 0.274	0.585 ± 0.020	0.107 ± 0.032	0.09	35
W_r^{gr}	RRab	-3.347 ± 0.404	0.241 ± 0.021	0.019 ± 0.047	0.10	31
	RRab+RRc	-3.178 ± 0.303	0.240 ± 0.022	0.042 ± 0.036	0.10	35
W_g^{gi}	RRab	-3.169 ± 0.362	0.435 ± 0.019	0.055 ± 0.042	0.09	31
	RRab+RRc	-2.987 ± 0.273	0.433 ± 0.019	0.078 ± 0.032	0.09	35
(geometric distances):						
g	RRab	-0.389 ± 0.617	0.792 ± 0.029	0.267 ± 0.070	0.15	31
	RRab+RRc	-0.217 ± 0.447	0.790 ± 0.029	0.285 ± 0.054	0.15	35
r	RRab	-1.092 ± 0.509	0.650 ± 0.024	0.208 ± 0.058	0.12	31
	RRab+RRc	-0.950 ± 0.371	0.648 ± 0.024	0.223 ± 0.045	0.12	35
i	RRab	-1.544 ± 0.461	0.633 ± 0.022	0.177 ± 0.053	0.11	31
	RRab+RRc	-1.402 ± 0.338	0.632 ± 0.022	0.193 ± 0.041	0.11	35
W_r^{ri}	RRab	-2.923 ± 0.393	0.583 ± 0.019	0.085 ± 0.045	0.09	31
	RRab+RRc	-2.824 ± 0.300	0.580 ± 0.019	0.096 ± 0.036	0.10	35
W_r^{gr}	RRab	-3.135 ± 0.430	0.237 ± 0.020	0.036 ± 0.049	0.10	31
	RRab+RRc	-3.124 ± 0.327	0.236 ± 0.021	0.040 ± 0.039	0.11	35
W_g^{gi}	RRab	-3.016 ± 0.388	0.431 ± 0.018	0.063 ± 0.044	0.09	31
	RRab+RRc	-2.955 ± 0.297	0.429 ± 0.019	0.071 ± 0.036	0.10	35
(photo-geometric distances):						
g	RRab	-0.473 ± 0.623	0.791 ± 0.030	0.257 ± 0.072	0.15	31
	RRab+RRc	-0.260 ± 0.456	0.789 ± 0.029	0.280 ± 0.055	0.15	35
r	RRab	-1.177 ± 0.525	0.650 ± 0.025	0.198 ± 0.060	0.13	31
	RRab+RRc	-0.993 ± 0.382	0.647 ± 0.024	0.218 ± 0.046	0.12	35
i	RRab	-1.629 ± 0.478	0.633 ± 0.023	0.168 ± 0.054	0.11	31
	RRab+RRc	-1.445 ± 0.349	0.631 ± 0.022	0.188 ± 0.042	0.11	35
W_r^{ri}	RRab	-3.008 ± 0.411	0.582 ± 0.019	0.075 ± 0.047	0.10	31
	RRab+RRc	-2.835 ± 0.299	0.580 ± 0.019	0.095 ± 0.036	0.10	35
W_r^{gr}	RRab	-3.220 ± 0.450	0.236 ± 0.021	0.026 ± 0.051	0.11	31
	RRab+RRc	-3.135 ± 0.328	0.236 ± 0.021	0.039 ± 0.040	0.11	35
W_g^{gi}	RRab	-3.101 ± 0.408	0.430 ± 0.019	0.054 ± 0.047	0.10	31
	RRab+RRc	-2.967 ± 0.296	0.430 ± 0.019	0.070 ± 0.036	0.10	35

Notes. band: the Pan-STARRS $g_{p1}r_{p1}i_{p1}$ bands and Wesenheit indicates constructed using reddening vectors from Green et al. (2019); type: variability type of RR Lyr star; a_λ : slope of the fit; b_λ : zero point of the fit; c_λ : metallicity coefficient; rms: a root mean square of derived relations; N: number of stars used for fitting. Pivot logarithm used for fitting was $\log P_0 = -0.25$ for RRab and RRab+RRc stars. Pivot metallicity values was chosen to be $[\text{Fe}/\text{H}]_0 = -1.5$. Fundamentalization according to Iben (1974): $\log P_{\text{ab}} = \log P_c + 0.127$.

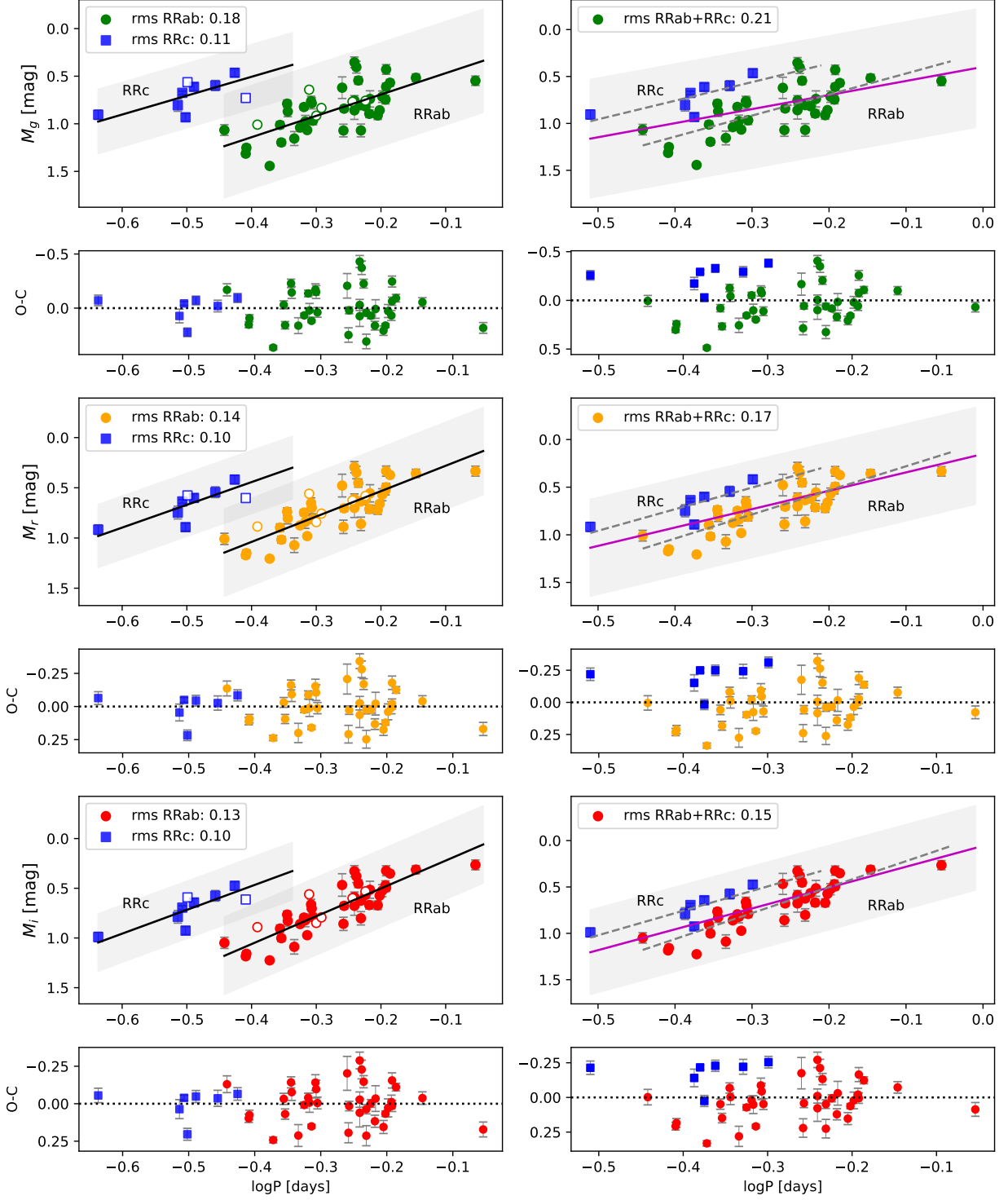


Fig. 2. PL relations for RR Lyr stars (RRab+RRC) based on mean reddenings from Schlafly & Finkbeiner (2011), the reddening vector (R_λ) from Green et al. (2019), and Gaia DR3 parallaxes. Filled circles and squares mark RRab and RRC stars adopted for derivation of the PL relations, respectively; open circles and squares: RRab and RRC stars with $RUWE > 1.4$, respectively; black solid and dashed gray lines: the fit to Equation (4) for RRab and RRC, separately; magenta solid line: the fit to Equation (4) for RRab+RRC stars; shaded areas: ± 3 rms.

Tonry, J. L., Stubbs, C. W., Lykke, K. R., et al. 2012, *ApJ*, 750, 99
 van der Walt, S., Colbert, S. C., & Varoquaux, G. 2011, *Computing in Science and Engineering*, 13, 22
 Virtanen, P., Gommers, R., Oliphant, T. E., et al. 2020, *Nature Methods*, 17, 261
 Vivas, A. K., Saha, A., Olsen, K., et al. 2017, *AJ*, 154, 85
 Wielgórski, P., Pietrzyński, G., Pilecki, B., et al. 2022, *The Astrophysical Journal*, 927, 89
 Zgirski, B., Pietrzyński, G., Górski, M., et al. 2023, *ApJ*, 951, 114

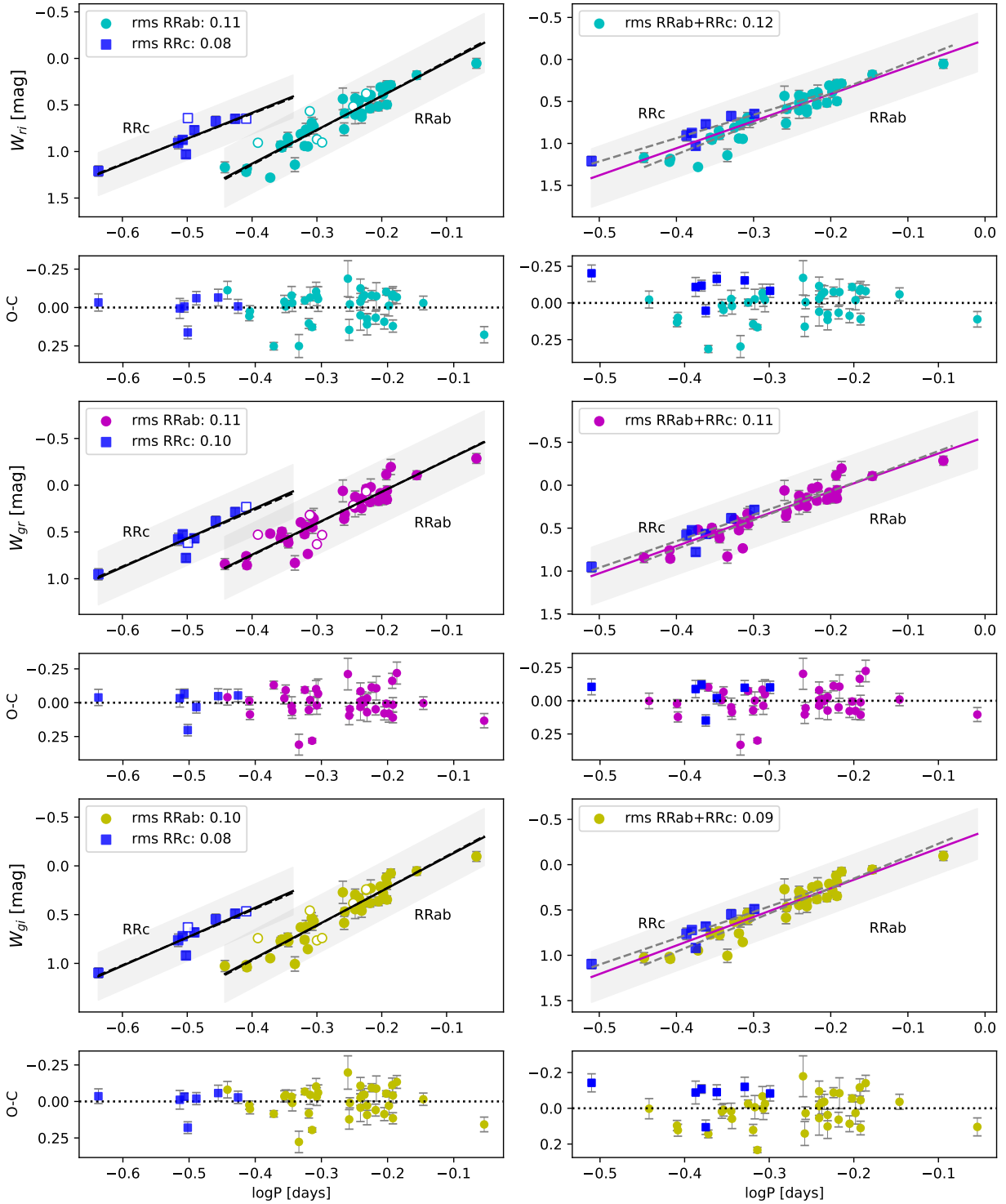


Fig. 3. PW relations for RR Lyr stars (RRab+RRc) based on mean reddenings from Schlafly & Finkbeiner (2011), the reddening vector (R_λ) from Green et al. (2019) and Gaia DR3 parallaxes. Filled circles and squares mark RRab and RRC stars adopted for derivation of the PW relations, respectively; open circles and squares: RRab and RRC stars with $RUWE > 1.4$, respectively; black solid and dashed gray lines: the fit to Equation (6) for RRab and RRC, separately; magenta solid line: the fit to Equation (4) for RRab+RRc stars; shaded areas: ± 3 rms.

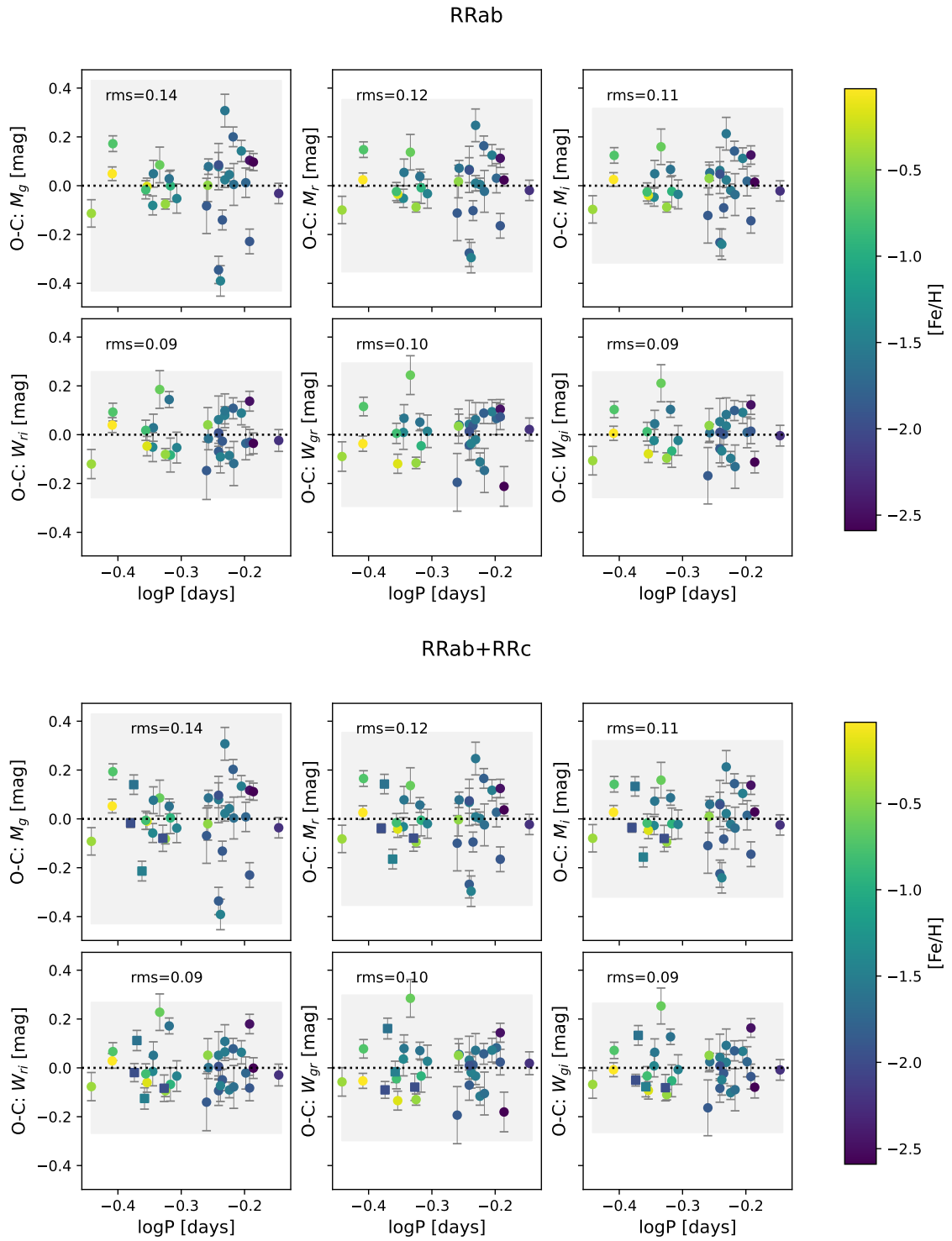


Fig. 4. Residuals of the PLZ and PWZ relations for the Sloan gri bands and Wesenheit indices for RR Lyr stars (RRab and RRab+RRc) based on the parallax method. Circles mark RRab stars; squares: RRc stars; shaded areas: ± 3 rms.

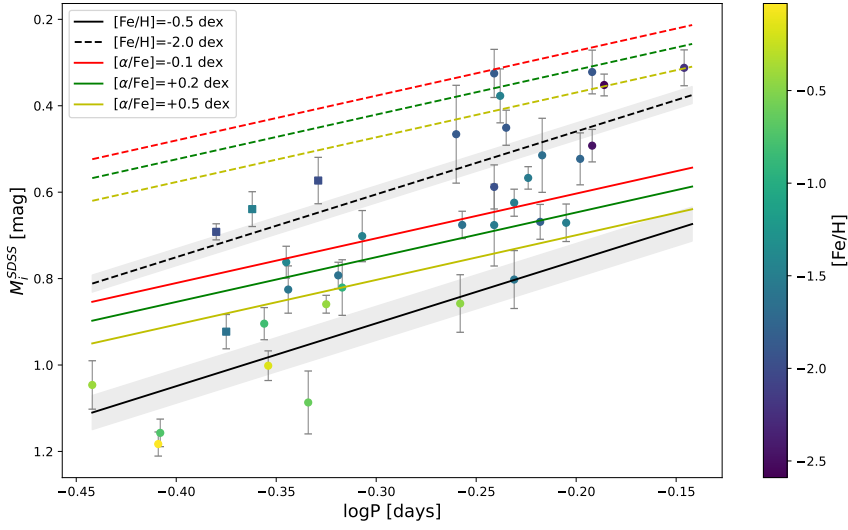


Fig. 5. Comparison of the PLZ relation derived in this work with the theoretical PLZ relation provided by Cáceres & Catelan (2008). Black lines mark the PLZ relation derived in this work for a constant metallicity of $[\text{Fe}/\text{H}] = -0.5; -2.0$ dex; gray, shaded areas: metallicity slope $c_i \pm \delta c_i$ from Equation 8; red, green, yellow lines: theoretical PLZ relation from Cáceres & Catelan (2008) for $[\alpha/\text{Fe}] = -0.1; +0.2; +0.5$ dex at a constant metallicity of $[\text{Fe}/\text{H}] = -0.5; -2.0$ dex.

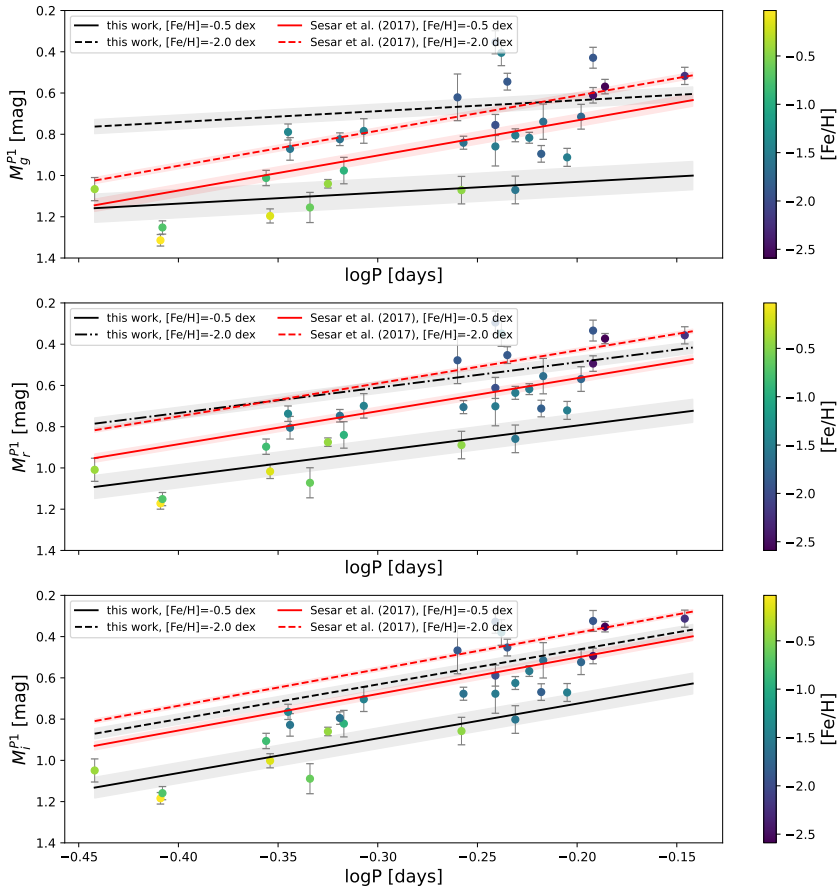


Fig. 6. Comparison of the PLZ relations derived in this work with empirical PLZ relations provided by Sesar et al. (2017). Black lines mark the PLZ relations derived in this work for a constant metallicity of $[\text{Fe}/\text{H}] = -0.5; -2.0$ dex; gray, shaded areas: metallicity slope $c_\lambda \pm \delta c_\lambda$ from Equation 8; red lines: empirical PLZ relation from Sesar et al. (2017) for a constant metallicity of $[\text{Fe}/\text{H}] = -0.5; -2.0$ dex; red, shaded areas: metallicity slope $\beta \pm \delta\beta$ from Table 1 in Sesar et al. (2017).

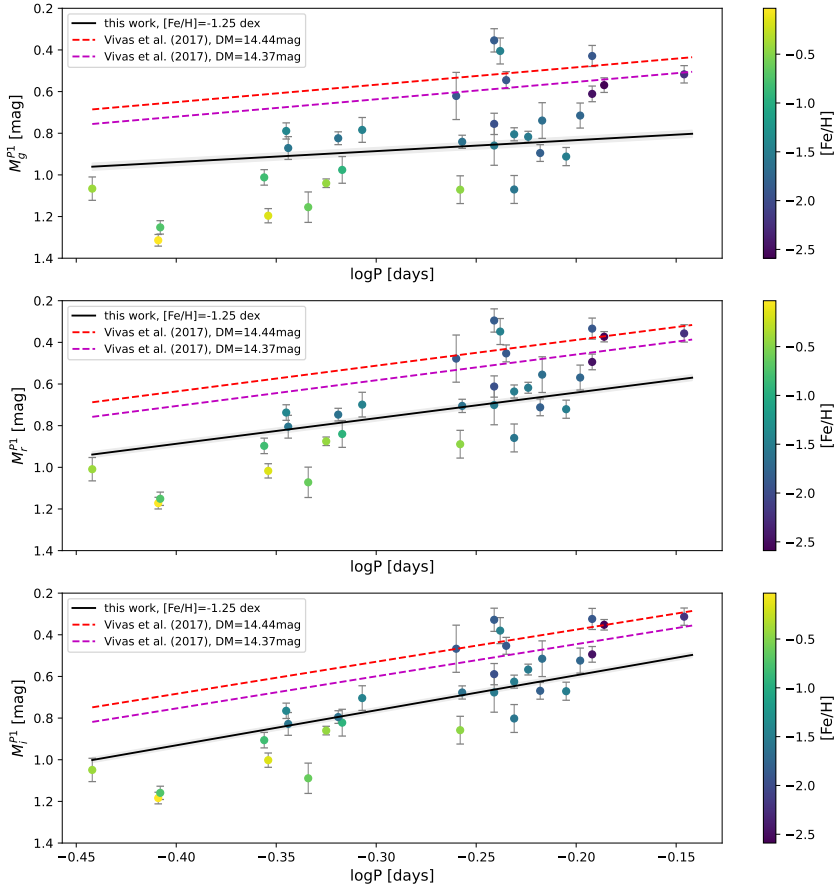


Fig. 7. Comparison of the PLZ relations derived in this work with empirical PLZ relations provided by Vivas et al. (2017) for the globular cluster M5. Comparison is given for two distances to M5. Black lines: the PLZ relations derived in this work for a constant metallicity of $[Fe/H] = -1.25$ dex; gray, shaded areas: metallicity slope $c_\lambda \pm \delta c_\lambda$ from Equation (8); red lines: empirical PLZ relation from Vivas et al. (2017) for a constant metallicity of $[Fe/H] = -1.25$ dex and distance modulus equal to 14.44 mag; magenta lines: same as red lines but for distance modulus equal to 14.37 mag from Table 1 of Baumgardt & Vasiliev (2021).

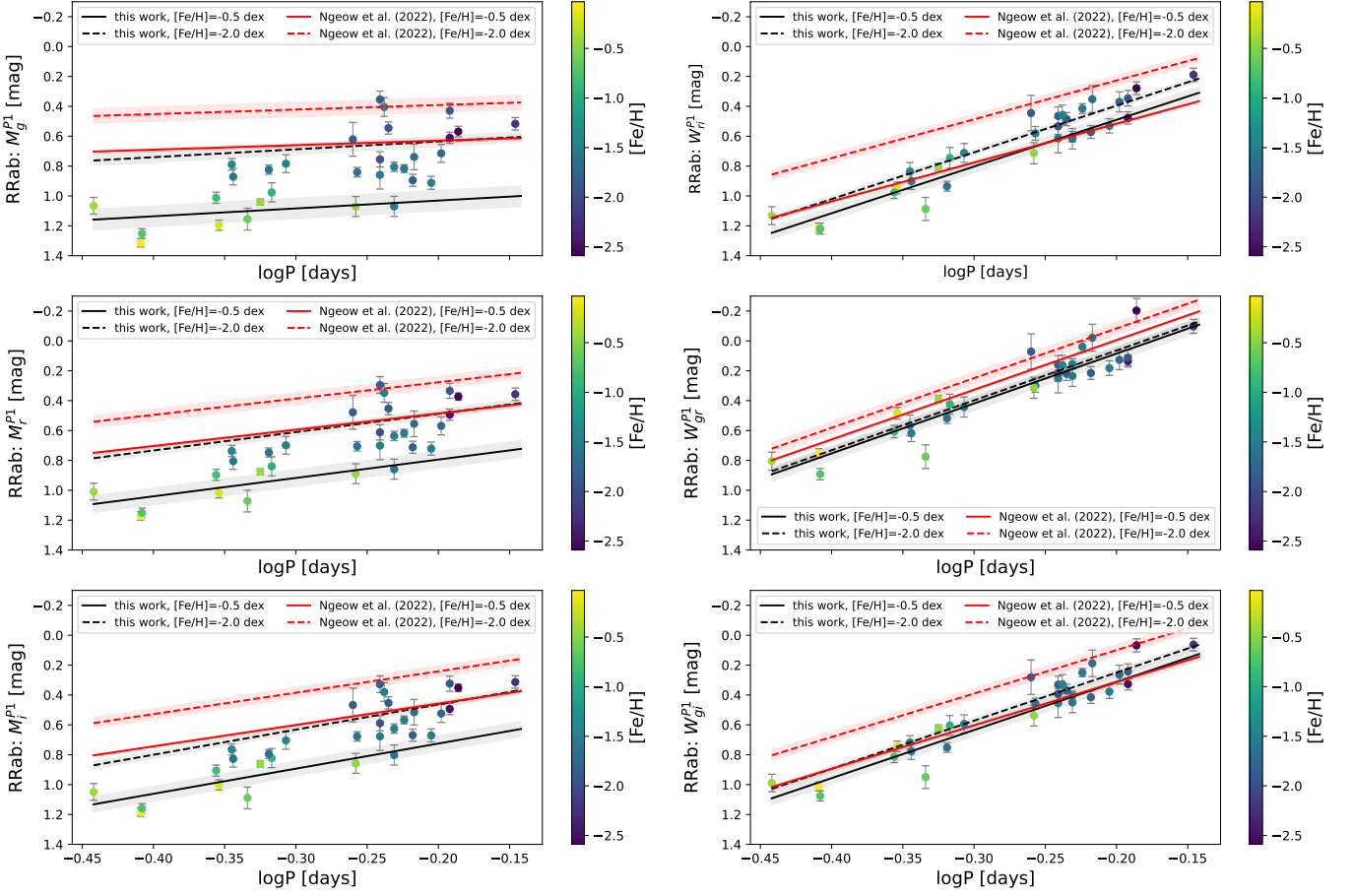


Fig. 8. Comparison of the PLZ and PWZ relations derived in this work with empirical PLZ and PWZ relations provided by Ngeow et al. (2022) from RR Lyr in 46 globular clusters. Black lines mark the PLZ and PWZ relations derived in this work for a constant metallicity of $[\text{Fe}/\text{H}] = -0.5; -2.0$ dex; gray, shaded areas: metallicity slope $c_\lambda \pm \delta c_\lambda$ from Equation (8); red lines: empirical PLZ relation from Ngeow et al. (2022) for a constant metallicity of $[\text{Fe}/\text{H}] = -0.5; -2.0$ dex; red, shaded areas: metallicity slope $c \pm \delta c$ from Table 4 in Ngeow et al. (2022).

Table 4. Shifts of $\log P$ in the fundamentalization formula determined for RRc stars.

band	$\Delta \log P$ (mag)	band	$\Delta \log P$ (mag)
(parallax):		(geometric distances):	
g	0.296 ± 0.034	g	0.297 ± 0.036
r	0.247 ± 0.023	r	0.246 ± 0.025
i	0.223 ± 0.019	i	0.222 ± 0.020
W_r^{ri}	0.174 ± 0.013	W_r^{ri}	0.171 ± 0.014
W_r^{gr}	0.151 ± 0.015	W_r^{gr}	0.149 ± 0.015
W_g^{gi}	0.164 ± 0.012	W_g^{gi}	0.162 ± 0.013
(ABL method):		(photo-geometric distances):	
g	0.298 ± 0.035	g	0.294 ± 0.035
r	0.249 ± 0.023	r	0.244 ± 0.024
i	0.226 ± 0.019	i	0.220 ± 0.020
W_r^{ri}	0.178 ± 0.012	W_r^{ri}	0.170 ± 0.014
W_r^{gr}	0.153 ± 0.014	W_r^{gr}	0.148 ± 0.016
W_g^{gi}	0.167 ± 0.012	W_g^{gi}	0.161 ± 0.013

Notes. band: the Sloan–Pan-STARRS $g_{p1}r_{p1}i_{p1}$ bands and Wesenheit indices; $\Delta \log P$: a new shift of $\log P$ for fundamentalization.

Appendix A: The Sloan band light curves of Galactic RR Lyr stars analyzed in this work

Figure A.1 presents the Sloan–Pan–STARSS $g_{P1}r_{P1}i_{P1}$ bands light curves of 44 RRab stars used in this study. Figure A.2 shows the analogous light curves for nine RRc stars. The figures are also available at Zenodo data repository: <https://doi.org/10.5281/zenodo.11565605>. The presented light curves are available at the webpage of the Araucaria Project: <https://araucaria.camk.edu.pl/> and the CDS.

Appendix B: The ZP shift of PL relations

Tables B.1 and B.2 present the ZP shift between PL relations obtained in this work with four methods of deriving absolute magnitudes described in Section 2.4, and theoretical and empirical PL relations from the literature.

Table B.1. ZP shift from the comparison with the theoretical PLZ relation from Cáceres & Catelan (2008).

$[\alpha/\text{Fe}]$ (dex)	parallax	ABL method	geometric distances	photo-geometric distances
$[\text{Fe}/\text{H}]_a = -0.5$ dex; $\log P_a = -0.25$ days				
-0.1	0.176	0.177	0.170	0.164
+0.2	0.132	0.133	0.126	0.120
+0.5	0.080	0.081	0.074	0.068
$[\text{Fe}/\text{H}]_a = -2.0$ dex; $\log P_a = -0.25$ days				
-0.1	0.207	0.210	0.209	0.210
+0.2	0.163	0.166	0.165	0.166
+0.5	0.111	0.114	0.113	0.114

Notes. The ZP shifts were calculated for PLZ relations of RRab+RRc stars, for adopted iron abundance $[\text{Fe}/\text{H}]_a$, constant period $\log P_a$ for filter SSSD*s*.

Table B.2. ZP shift from the comparison with empirical PLZ relations.

Sesar et al. (2017)				
filter	parallax	ABL method	geometric distances	photo-geometric distances
$[\text{Fe}/\text{H}]_a = -0.5$ dex; $\log P_a = -0.25$ days				
M_g^{P1} (RRab)	0.241	0.247	0.242	0.231
M_r^{P1} (RRab)	0.211	0.214	0.213	0.203
M_i^{P1} (RRab)	0.219	0.223	0.220	0.211
$[\text{Fe}/\text{H}]_a = -2.0$ dex; $\log P_a = -0.25$ days; M_i				
$[\alpha/\text{Fe}]$ (dex)	parallax	ABL method	geometric distances	photo-geometric distances
M_g^{P1} (RRab)	-0.036	-0.033	-0.039	-0.035
M_r^{P1} (RRab)	0.039	0.043	0.036	0.041
M_i^{P1} (RRab)	0.078	0.081	0.075	0.079
Vivas et al. (2017)				
$[\text{Fe}/\text{H}]_a = -1.25$ dex (M5); $\log P_a = -0.25$ days; $\text{DM}_a = 14.44$ mag				
M_g^{P1} (RRab)	0.335	0.339	0.334	0.330
M_r^{P1} (RRab)	0.252	0.256	0.252	0.249
M_i^{P1} (RRab)	0.226	0.229	0.225	0.223
$[\text{Fe}/\text{H}]_a = -1.25$ dex (M5); $\log P_a = -0.25$ days; $\text{DM}_a = 14.37$ mag				
M_g^{P1} (RRab)	0.265	0.269	0.264	0.260
M_r^{P1} (RRab)	0.182	0.186	0.182	0.179
M_i^{P1} (RRab)	0.156	0.159	0.155	0.153
Bhardwaj et al. (2021)				
$[\text{Fe}/\text{H}]_a = -2.33$ dex (M15); $\log P_a = -0.25$ days; $\text{DM}_a = 15.15$ mag				
M_g^{SSS} (RRab)	0.174	0.176	0.170	0.177
M_r^{SSS} (RRab)	0.210	0.213	0.206	0.213
M_i^{SSS} (RRab+RRc)	0.179	0.182	0.181	0.185
M_i^{SSS} (RRab+RRc)	0.197	0.200	0.200	0.203
Ngeow et al. (2022)				
$[\text{Fe}/\text{H}]_a = -0.5$ dex; $\log P_a = -0.25$ days				
M_g^{P1} (RRab)	0.413	0.419	0.414	0.403
M_r^{P1} (RRab)	0.316	0.319	0.318	0.308
M_i^{P1} (RRab)	0.280	0.284	0.281	0.272
W_g^{P1} (RRab)	0.019	0.024	0.021	0.010
W_r^{P1} (RRab)	0.111	0.099	0.112	0.101
W_{gi}^{P1} (RRab)	0.035	0.032	0.036	0.026
M_g^{P1} (RRab+RRc)	0.366	0.371	0.361	0.355
M_r^{P1} (RRab+RRc)	0.304	0.305	0.297	0.291
M_i^{P1} (RRab+RRc)	0.299	0.300	0.293	0.287
W_g^{P1} (RRab+RRc)	0.060	0.068	0.052	0.051
W_r^{P1} (RRab+RRc)	0.198	0.192	0.186	0.185
W_{gi}^{P1} (RRab+RRc)	0.085	0.083	0.072	0.072
$[\text{Fe}/\text{H}]_a = -2.0$ dex; $\log P_a = -0.25$ days				
M_g^{P1} (RRab)	0.255	0.258	0.252	0.256
M_r^{P1} (RRab)	0.217	0.221	0.214	0.219
M_i^{P1} (RRab)	0.235	0.238	0.232	0.236
W_g^{P1} (RRab)	0.186	0.188	0.184	0.188
W_r^{P1} (RRab)	0.150	0.148	0.136	0.140
W_{gi}^{P1} (RRab)	0.158	0.163	0.154	0.158
M_g^{P1} (RRab+RRc)	0.218	0.221	0.219	0.220
M_r^{P1} (RRab+RRc)	0.194	0.197	0.195	0.196
M_i^{P1} (RRab+RRc)	0.176	0.177	0.176	0.177
W_g^{P1} (RRab+RRc)	0.130	0.131	0.131	0.132
W_r^{P1} (RRab+RRc)	0.138	0.144	0.141	0.142
W_{gi}^{P1} (RRab+RRc)	0.116	0.118	0.118	0.119

Notes. The shifts were calculated for adopted iron abundance $[\text{Fe}/\text{H}]_a$, constant period $\log P_a$.

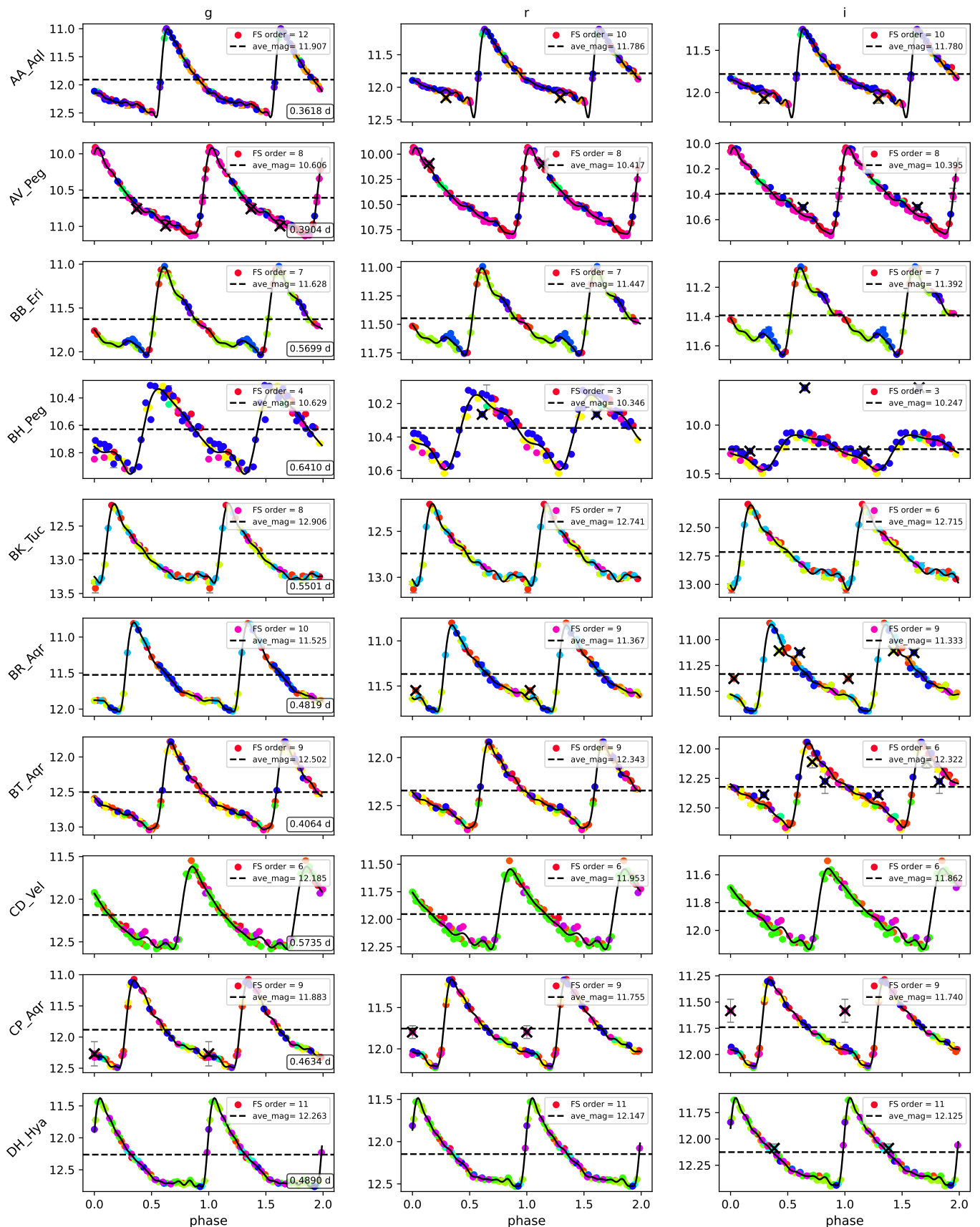


Fig. A.1. Sloan–Pan–STARRS $g_{P1}r_{P1}i_{P1}$ band light curves of RRab stars analyzed in this work. Horizontal dashed, black lines correspond to the determined mean magnitudes. Different colors of points mark different telescopes used during the data collection, while black crosses mark points rejected during the fitting. Black lines show the best fit Fourier series.

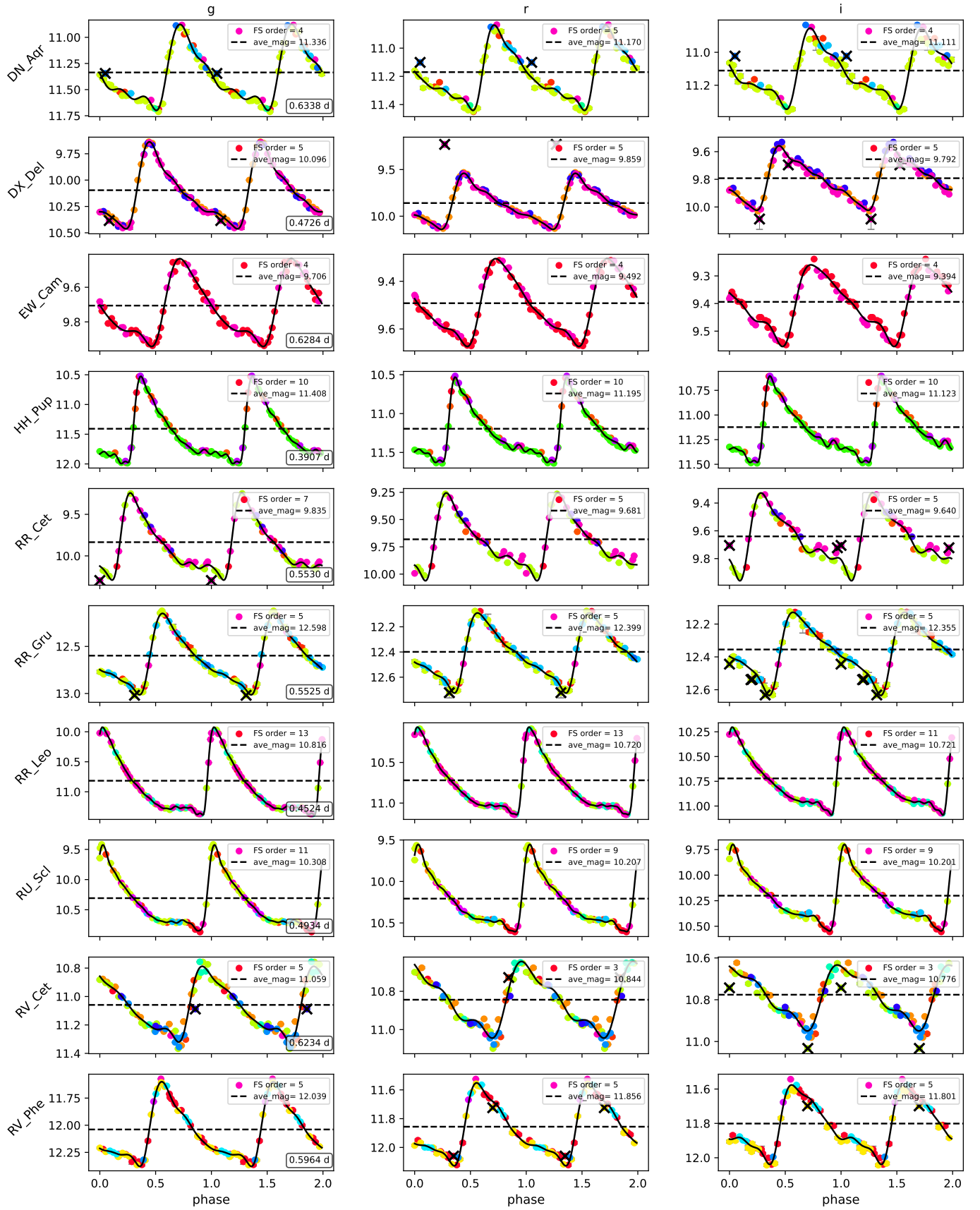


Fig. A.1. Continued from the previous page.

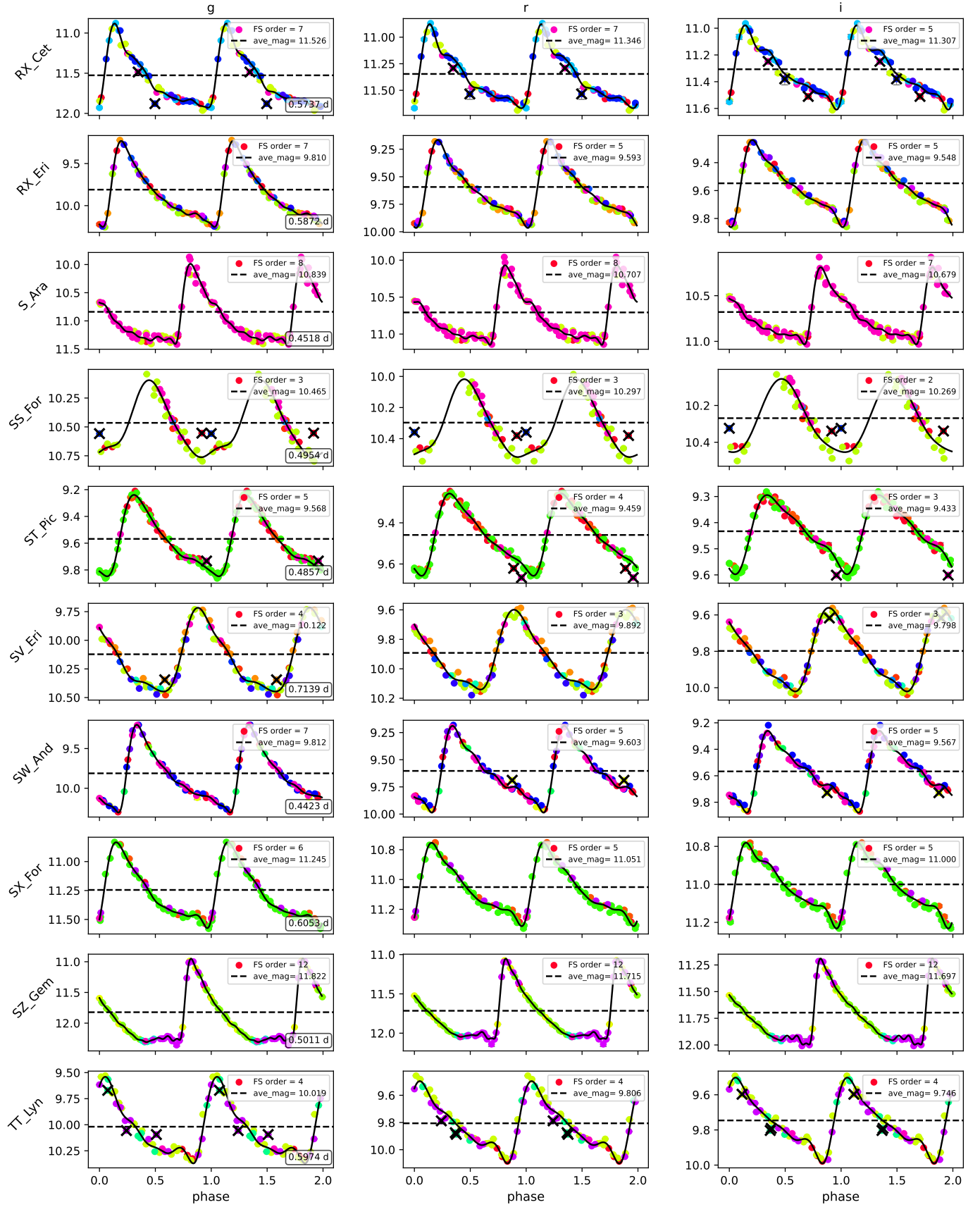


Fig. A.1. Continued from the previous page.

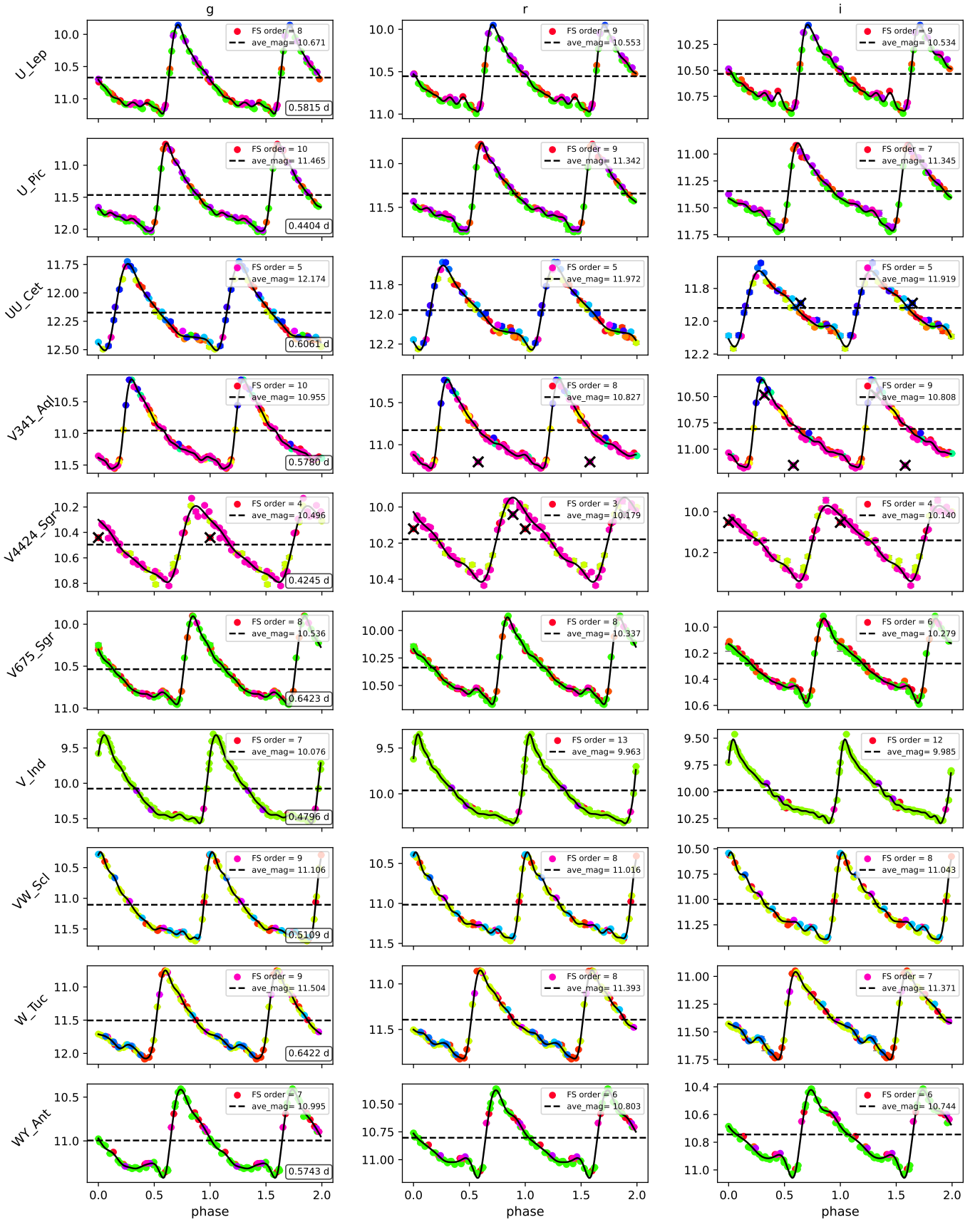


Fig. A.1. Continued from the previous page.

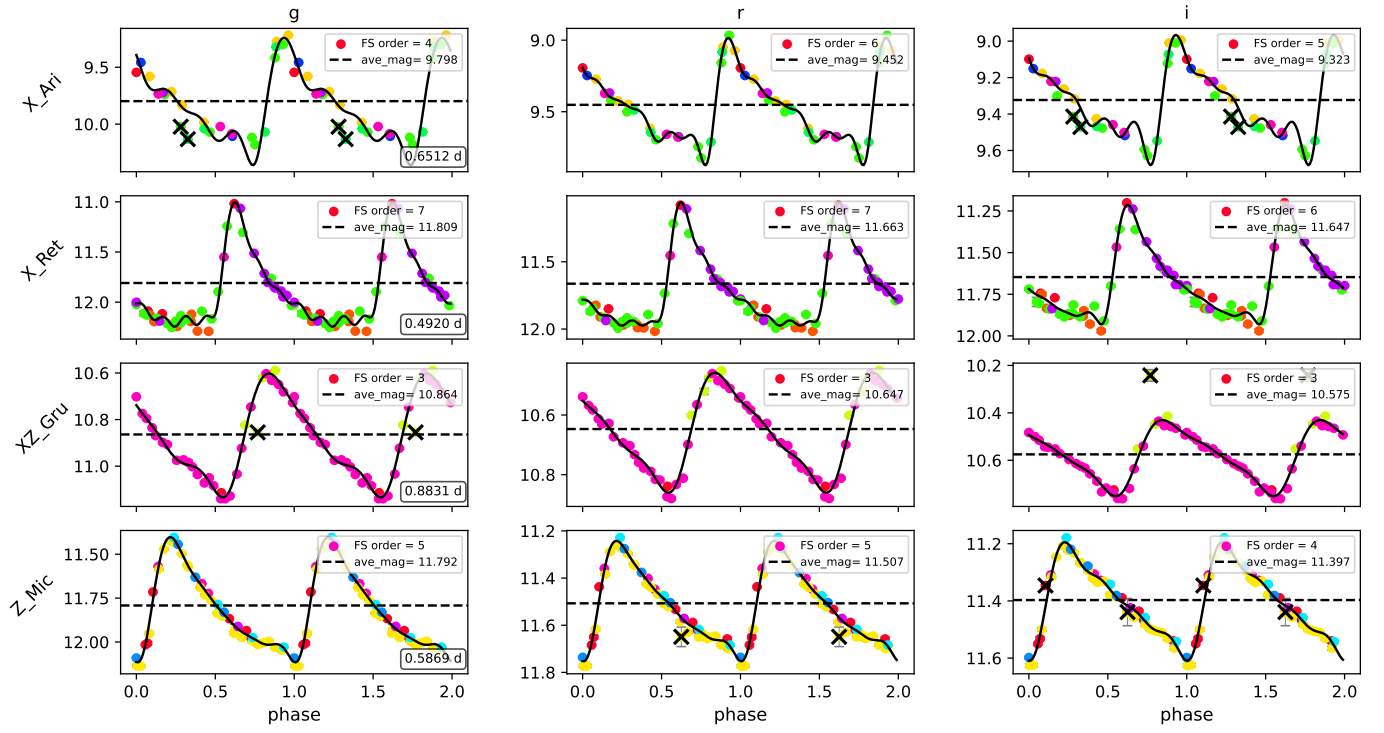


Fig. A.1. Continued from the previous page.

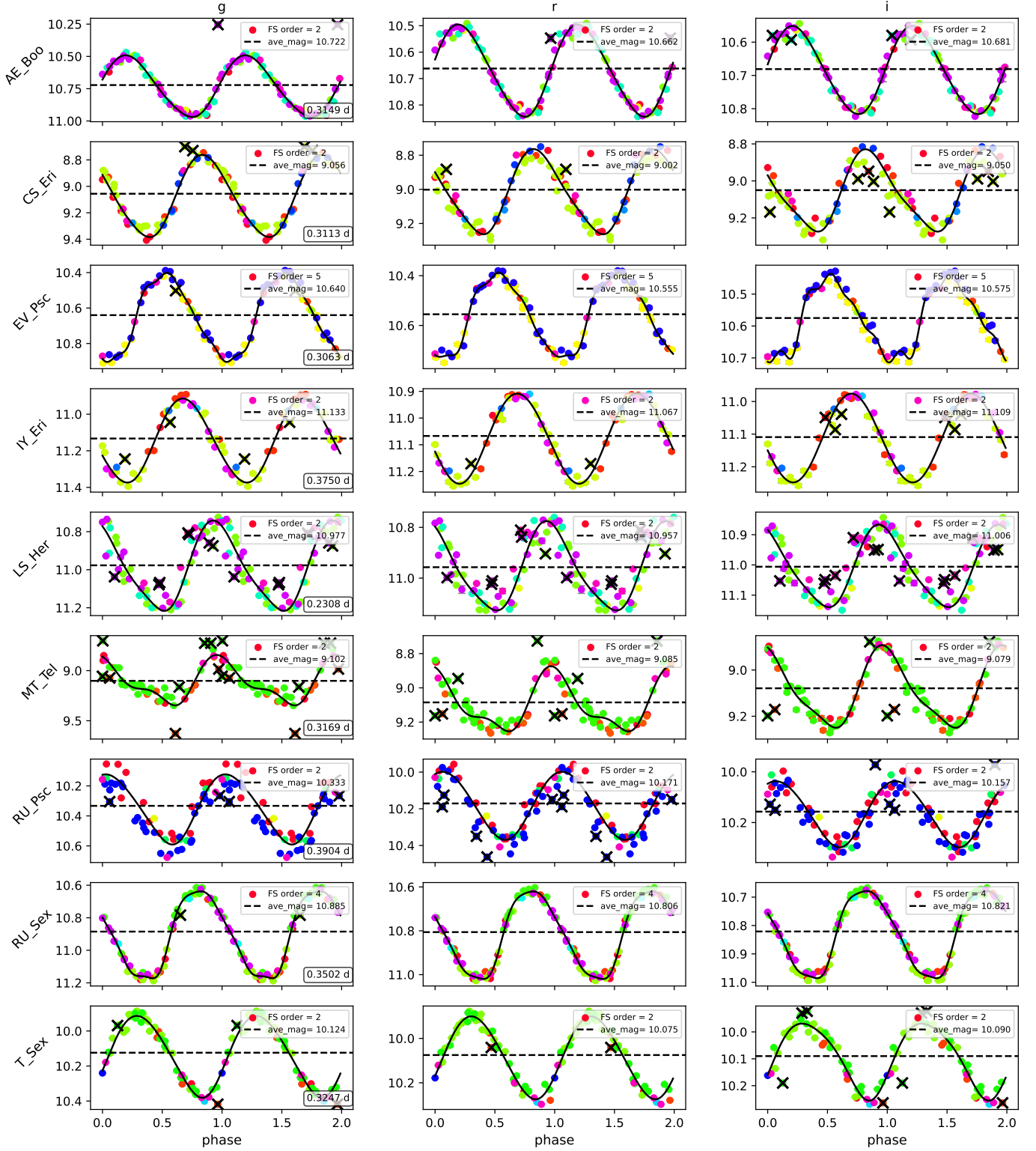


Fig. A.2. Sloan–Pan–STARRS $g_{p1}r_{p1}i_{p1}$ band light curves of RRc stars analyzed in this work. Horizontal dashed, black lines correspond to the determined mean magnitudes. Different colors of points mark different telescopes used during the data collection, while black crosses mark points rejected during the fitting. Black lines show the best fit Fourier series.